https://doi.org/10.5194/hess-2021-284
Preprint. Discussion started: 11 June 2021

Hydrology and Earth System Sciences
Open Access
EGU
Discussions

The contribution of transpiration, ground evaporation, and canopy evaporation to local and remote precipitation across North America

Tyler S. Harrington[1], Jesse Nusbaumer[2], Christopher B. Skinner[1]

[1]University of Massachusetts-Lowell, Department of Environmental, Earth, & Atmospheric Sciences, Lowell, MA, 01854, USA
[2]National Center for Atmospheric Research, Climate & Global Dynamics Laboratory, Boulder, CO, 80307, USA

Correspondence: Tyler S. Harrington (tyler_harrington2@student.uml.edu)

Abstract. Land surface evapotranspiration (ET) is a major source of moisture for the global hydrologic cycle. Though the influence of the land surface is well documented, moisture tracking analysis has often relied on offline tracking approaches that require simplifying assumptions and can bias results. Additionally, the contribution of the ET components (transpiration (T), canopy evaporation (C), and ground evaporation (E)) individually to precipitation is not well understood, inhibiting our understanding of moisture teleconnections in both the current and future climate. Here we use the Community Earth System Model version 1.2 with online numerical water tracers to examine the contribution of local and remote land surface ET, including the contribution from each individual ET component, to precipitation across North America. We find the role of the land surface and the individual ET components varies considerably across the continent and across seasons. Much of northern and northeastern North America receives up to 80% of summertime precipitation from land surface ET, and over 50% of that moisture originates from transpiration alone. Local moisture recycling constitutes an essential source of precipitation across much of the southern and western regions of North America, while remote land surface moisture supplies most of the land-based precipitation across northern and eastern North America. Though the greatest contribution of remotely sourced land ET occurs in the north and east, we find the primary sources of North American land surface moisture shifts seasonally. The results highlight regions that are especially sensitive to land cover and hydrologic changes in local and upwind areas, providing key insights for drought prediction and water resource management.

1. Introduction:

Evapotranspiration (ET) from the land surface is a major atmospheric moisture source responsible for approximately 35% of precipitation over land (van der Ent et al., 2014). This terrestrial-sourced moisture is supplied by advection of ET from upwind land surfaces (moisture transport) and by ET from within the land region of interest (moisture recycling). Regions that rely heavily on terrestrial ET moisture for precipitation are susceptible to mechanisms that alter land surface ET such as land use and land cover change (Weng et al., 2018; Paul et al., 2016; Alter et al., 2017). Additionally, the degree to which a region depends on local recycled moisture influences the development of land surface feedbacks that can mitigate or exacerbate dry and wet periods, including high-impact drought and flood events (Dirmeyer and Brubaker, 1999; Seneviratne et al. 2010; Kelemen et al., 2016). It is therefore critical to understand the breakdown of a region's terrestrial moisture sources, including the contributions from moisture transport and recycling, and the contributions from different land cover types, such as vegetation and soil, for water resource management.

Previous studies have identified terrestrial ET as an important source of moisture for North American precipitation. For example, van der Ent et al. (2010) used reanalysis data and an atmospheric moisture budget-based accounting model to quantify a continental precipitation recycling ratio and found that terrestrial ET is responsible for approximately 40% of annual precipitation across most of the North American continent (van der Ent et al., 2010). The authors also quantified the continental evaporation recycling ratio and found that nearly 60% of evaporated moisture from the western half of North America falls as precipitation over land (van der Ent et al., 2010). Both the continental precipitation recycling ratio and the continental evaporation recycling ratio are projected to decrease across North America with future warming, highlighting the sensitivity of moisture source-sink relationships to varying environmental conditions, and the need to understand the underlying processes that influence these relationships to confidently predict future water availability (Findell et al. 2019).

While the continental recycling ratios point to a key role for the land surface as a whole in shaping North American precipitation, within this continental-scale framework, all precipitation sourced from the land surface is considered "recycled" even though it might have evaporated thousands of kilometers upwind. A regional-scale recycling framework is necessary to identify the contribution of proximate and remote terrestrial sources to precipitation. Though the definition of "regional scale" within the context of moisture recycling is subjective and influences the quantity of recycled precipitation (Dirmeyer and Brubaker, 2007; Singh et al. 2016), the overlying goal of the framework is to gain an understanding of how reliant a region is on ET from the surrounding area. This knowledge can assist in understanding the role of land surface feedbacks within the context of atmospheric events such as droughts, floods, and heat waves (Raddatz, 2005; Roy et al., 2019; Miralles et al., 2019), and in local land use/land cover decision making. For example, previous work has found that changes to crop management practices, such as a reduction in irrigation in California's Central Valley, would reduce precipitation in California and the surrounding Southwest U.S. (Lo and Famiglietti, 2013). Changes to land use and agricultural practices in the Central Valley should therefore be considered carefully to limit potential adverse regional hydroclimate impacts.

In addition to knowing the geographic sources of a region's precipitation, identification of the surfaces from which that terrestrial ET is sourced can further enhance understanding of regional hydroclimate and assist water resource management. Land surface ET is a combination of transpiration (T), canopy evaporation (C), and ground evaporation (E). The T component alone accounts for nearly 64% of total global ET (Good et al., 2015), making vegetation critical for land moisture recycling. However, the degree to which a region relies

https://doi.org/10.5194/hess-2021-284
Preprint. Discussion started: 11 June 2021

on T for precipitation depends on proximity to dense, high-transpiration plants, and/or alignment to the prevailing winds that flow over those plants (Keys et al. 2016). Regions that rely more heavily on T may exhibit less variability in precipitation than regions that rely largely on C or E, as plants with deep rooting systems are able to tap into water deep below ground providing moisture to the atmosphere even during relatively dry periods (Tueling et al., 2010; Lee et al., 2012). T moisture has also been shown to have a longer average atmospheric residence time than moisture from C or E (van der Ent et al., 2014). Given differing magnitudes and residence times of the three ET components, examining each components' role in precipitation and local recycling individually is necessary for a complete understanding of the hydrologic cycle.

Additionally, there is much uncertainty regarding the partitioning of ET in future climates (Kirschbaum, 2004). Some studies have suggested increased leaf-area index (LAI) and a lengthened growing season will result in an increase in T (Niu et al., 2019), while other studies have found CO2 fertilization decreases T (Kirschbaum & McMillan, 2018). The uncertainty surrounding ET partitioning in future climates adds to the uncertainty in moisture recycling patterns as well. Having a clear understanding of moisture recycling and the contribution of each ET component in the current climate is necessary for future water resource planning.

Here we present a new unified framework to study regional moisture recycling and the sourcing of precipitation into its individual ET components (T, E, and C). Using a climate model with water tracing capability, we identify the reliance of each location in North America on precipitation sourced from transpiration, canopy evaporation, and soil/lake surface evaporation, highlighting regions most susceptible to changes in vegetation type, coverage, and physiology. We then estimate precipitation recycling on a regional scale, providing an assessment of precipitation sensitivity to local and remote land use/land cover changes (whether land management-or climate-driven). Lastly, we combine the water tracing analyses to quantify the breakdown of local and remote terrestrial moisture recycling into the T, E, and C components.

2. Methods:

2.1 Model Setup

We utilize the isotope-enabled Community Earth System Model version 1.2 (iCESM1.2) (Hurrell et al., 2013; Brady et al., 2019). The model is configured with the Community Atmosphere Model version 5 (CAM5) and the Community Land Model version 5 with prognostic vegetation state and active biogeochemistry (CLM5BGC). Both CAM5 and CLM5 are run on a 0.9° x 1.25° finite volume grid. CAM5 is run with 30 active atmospheric levels in a hybrid-sigma pressure coordinate system. Crop management and irrigation are active within CLM5. The ocean is initialized and forced with prescribed monthly-varying sea-surface temperatures (SSTs) and sea-ice concentrations (SICs) from the

https://doi.org/10.5194/hess-2021-284
Preprint. Discussion started: 11 June 2021

Hadley Centre Global Sea Ice and Sea Surface Temperature (HadISST) dataset (Rayner et al., 2003). The model is run for 31 years using SSTs, SICs, greenhouse gas concentrations, and aerosols consistent with the years 1985-2015. For the years 2006-2015, greenhouse gas concentrations and aerosols are taken from the Representative Concentration Pathway 4.5 (RCP4.5) (Thomson et al., 2011). The first year of the simulation (1985) is discarded to allow the water tracers to spin-up (see below), leaving a 30-year climatology.

Our configuration of CESM utilizes the online water tracing capability of CAM5 (Brady et al., 2019; Nusbaumer and Noone, 2018). The water tracers allow for the tagging of water vapor evaporated from predefined land and ocean surfaces. The model "tags" moisture from regions with a unique identifier based on the region it evaporated from. The tagged water vapor is advected through the atmosphere in the same manner as regular water vapor and is subjected to all of the same physical processes including all cloud microphysics, boundary layer processes, and convection. The tagged moisture is tracked in the model through all atmospheric processes until the tagged moisture precipitates. The water tracers are passive and do not alter the state of the climate in any way, so an arbitrary number of them can be implemented into the model. By utilizing the water tracing capabilities of CAM5, we are able to directly quantify the sources of precipitation and the amount of moisture recycling that occurs in any predefined region. The online numerical water tracers also avoid the need for simplifying assumptions about the sub-grid processes that the tagged moisture undergoes. Many offline tracking methods including Lagrangian back-trajectory analyses and two-dimensional analytical models rely on simplifying assumptions about the state of the atmosphere such as the "well-mixed" atmosphere that can bias moisture source origins (Sodemann et al. 2008; van der Ent et al., 2013).

Additionally, we have extended the water tracing capabilities of CAM5 to include the tracing of the individual components of terrestrial ET (T, C, and E). The T tracers track all moisture originating from transpiration, the C tracers track moisture evaporated from the surface of plants, and the E tracers track all moisture evaporated from ground and lake surfaces, excluding evaporation or sublimation from surface snow. This added tracing capability allows for the direct quantification of precipitation from T, C, and E individually from each defined land region. There are a total of 22 defined land regions (Figure 1), each with 4 separate water tracers (ET, T, C, and E), for a total of 88 active water tracers for the North American land surface.

Figure 1: The defined land regions in the study. Each land region has 4 tracers: total ET, T, C, and E.

2.2 Mathematical Framework

In Sections 3.5 and 3.8, we examine the divergence of locally evaporated moisture and the convergence of remotely evaporated moisture for each defined land region across North America. We start with the fundamental equation of hydrology (Peixoto and Oort, 1992)

$$\frac{\partial Q}{\partial t} + \left(\nabla \cdot \tilde{Q}\right) = E - P \qquad (1)$$

where E is evaporation, P is precipitation, Q represents the column-integrated atmospheric moisture, and $\tilde{Q}$ represents the column-integrated moisture flux. It can be shown that for time periods greater than one year, the variability of atmospheric water storage is negligible (Singh et al., 2016; Dominguez et al., 2006). After integrating (1) globally,

$$\overline{E} = \overline{P} \qquad (2)$$

where the bars represent climatological averages. We utilize the mathematical framework developed by Singh et al. (2016) to transform equation (2) into

https://doi.org/10.5194/hess-2021-284
Preprint. Discussion started: 11 June 2021

$$P_i = E_i + \sum_{j=1, j\neq i}^{j=n} e_j f_{ji} E_j - E_i e_i \qquad (3)$$

where i and j denote individual domains smaller than the global domain, e denotes the export fraction (the fraction of evaporation that does not precipitate locally), and f_{ji} denotes the fraction of export from region j that falls in region i. This formulation of moisture conservation works for a global domain, i.e.

$$\sum_{i=1}^{i=n} \alpha(i) = \alpha(Globe)$$

where α represents the area, but requires an adjustment to work for a limited domain. For our study, we treat each defined land region as a subdomain of the North American land surface rather than the globe. In Appendix A, we show that for Equation (3) to hold on a restricted domain, it requires an adjustment such that

$$\ddot{P}_i = \ddot{E}_i + \left(\sum_{j=1, j\neq i}^{j=n} \ddot{e}_j f_{ji} \ddot{E}_j \right) - \ddot{E}_i \ddot{e}_i \qquad (4)$$

where $\ddot{\cdot}$ denotes scaled values so only moisture originating from and precipitating within the domain of interest is considered. Since we restrict our domain to the North American continent, only P originating from North America and E from North America that precipitates over North America are used in (4). Additionally, our e is restricted such that only moisture exported to other North American land regions is considered. Writing (4) in a matrix form for n regions leaves us with

$$\vec{\ddot{P}} = \vec{\ddot{E}} - (\mathbf{I} - \mathbf{F})\ddot{\mathbf{T}}\vec{\ddot{E}} \qquad (5)$$

where $\vec{\ddot{P}}$ and $\vec{\ddot{E}}$ are vectors of domain-scaled P and E of size n, $\mathbf{I}$ is the identity matrix, $\ddot{\mathbf{T}}$ is the domain-scaled export matrix with diagonal entries e_i and all non-diagonal entries equal to 0, and $\mathbf{F}$ is the convergence matrix with non-diagonal entries equal to f_{ji} and all diagonal entries equal to 0.

https://doi.org/10.5194/hess-2021-284
Preprint. Discussion started: 11 June 2021

2.3 GPCP Dataset

To evaluate CESM's ability to simulate North American precipitation, we compare CESM-simulated precipitation to rainfall observations from the Global Precipitation Climatology Project (GPCP) (Adler et al., 2020). The GPCP dataset consists of monthly rainfall estimates derived from a combination of in-situ gauge measurements and satellite observations. The GPCP data is stored on a 2.5° grid and is re-gridded to a 0.9° x 1.25° grid using patch interpolation to match that of CESM. GPCP rainfall estimates from the years 1986-2015 are used to create an observational climatology dataset to directly compare to the CESM precipitation climatology covering the same time period.

2.4 GLEAM Dataset

The CESM-simulated ET field is compared to the Global Land Evaporation Amsterdam Model (GLEAM) (Martens et al., 2017). The GLEAM dataset uses the Priestly and Taylor equation to calculate potential evaporation using observations of surface net-radiation, near-surface temperature, and surface soil moisture. GLEAM also incorporates satellite observations of vegetation optical depth (VOD) and calculates interception loss using a Gash Analytical Model. The dataset provides monthly estimates of total ET, T, and E on a 0.25° regular latitude-longitude grid. GLEAM evaporation estimates from the years 1986-2015 are re-gridded to a 0.9° x 1.25° grid using patch interpolation and averaged to create ET climatology files that can be directly compared to CESM.

3. Results:

3.1 Comparison of iCESM Precipitation to GPCP Observations

iCESM simulates precipitation reasonably well across North America, though there are notable differences between the iCESM and GPCP precipitation fields (Figure 2). During the winter, spring, and fall seasons, there is a broad area of positive precipitation anomalies across the eastern half of the United States indicating a deficit of iCESM precipitation compared to GPCP observations (Figures 2a, 2b, and 2d). The most significant positive anomalies are largely contained within our defined SCP and SSE regions. A weighted average of the anomalies over these two regions indicates an iCESM precipitation deficit of approximately 0.31, 0.14, and 0.35 mm day^-1 during the winter, spring, and fall seasons respectively. During the summer season, the region of positive precipitation anomalies largely shifts to the United States central plains (contained primarily within our SCP, ICP, INP, NMW, and RMW defined regions) (Figure 2c). A weighted average of the anomaly field over these five regions results in an average modeled precipitation deficit of 0.26 mm day^-1. Seasonal underestimations of precipitation in the southeastern US during the winter

https://doi.org/10.5194/hess-2021-284
Preprint. Discussion started: 11 June 2021

and in the central US during the summer are common amongst the 34 Coupled Model Intercomparison Project Phase 5 (CMIP5) models, and the error produced by iCESM is in line with other CMIP5 models (Sheffield et al., 2013). In contrast with much of eastern North America, iCESM generally overestimates precipitation across the western portions of the continent. The negative precipitation anomalies (indicating a surplus of modeled precipitation) are largely confined to the mountainous regions in all four seasons (Figure 2). These anomalous precipitation fields are likely the result of the model's resolved topography (Kopparla et al., 2013). Indeed, across CMIP5, models generally overestimate precipitation in regions with complex topography such as Western North America (Mehran et al., 2014). Though observational datasets like GPCP are often used to validate modeled precipitation fields, observations suffer from limited gauge data and limitations of satellite estimations, particularly within mountainous regions (Mehran and AghaKouchak, 2014; Sorooshian et al., 2011; Mehran et al., 2014). Some of the deviations between the iCESM and GPCP precipitation fields are likely the result of errors in the observational dataset rather than solely being a function of model error. Despite the slight model biases, iCESM resolves precipitation reasonably well across North America at a 1° resolution (Tapiador et al., 2017), and is an appropriate model to study North American precipitation characteristics.

https://doi.org/10.5194/hess-2021-284
Preprint. Discussion started: 11 June 2021

Hydrology and Earth System Sciences
Discussions

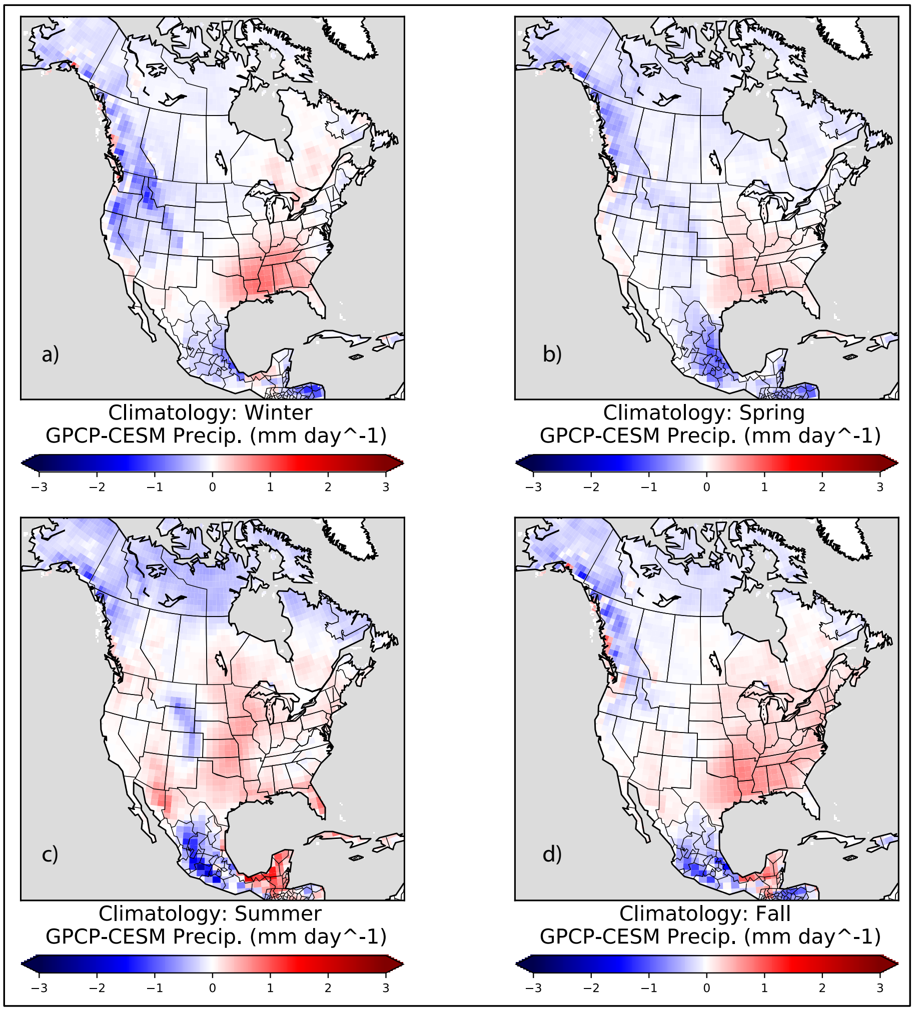

Figure 2. A comparison of the North American precipitation from iCESM and GPCP for (a) winter (DJF), (b) spring (MAM), (c) summer (JJA), and (d) fall (SON). Units are in mm day^-1.

3.2 Comparison of iCESM ET to GLEAM

Compared to GLEAM observations, iCESM simulates ET reasonably well across all four seasons (Figure 3). The maximum error (after taking the absolute value) between the two datasets is 0.61, 0.77, 0.70, and 0.56 mm day^-1 during the winter, spring, summer, and fall seasons respectively. On average, the model underestimates land surface ET in North America during the winter and fall seasons (Figures 3a & 3d). During the spring season, iCESM underestimates land surface ET across most of the northern half of North America, while overestimating ET in the southwestern US and Central America (Figure 3b). There is no clear spatial pattern in the ET error produced by iCESM during the summer season

https://doi.org/10.5194/hess-2021-284
Preprint. Discussion started: 11 June 2021

(Figure 3c). Though the maximum grid cell error occurs during the spring season, the average of the absolute value of the errors continent wide peaks in the summer (0.14 mm day^-1) compared to the winter (0.05 mm^day-1), spring (0.12 mm day^-1), and fall (0.08 mm day^-1) seasons. One potential source of error in climate model ET estimates is directly related to errors in the modeled precipitation (Mueller & Seneviratne, 2013). If precipitation is overestimated (underestimated) in the model, more (less) moisture is available for ET. Though the potential for this bias exists across the continent given the errors in modeled precipitation (Figure 2), this source of error appears most prominent in the US Southeast and in North-Central Mexico. In the US Southeast (in North-Central Mexico), iCESM underestimates (overestimates) precipitation in all four seasons (Figure 2), potentially resulting in underestimates (overestimates) of ET year-round (Figure 3). However, the sign of the precipitation and ET errors are not consistent spatially across all seasons, indicating other error sources are responsible for the disagreement between ET in the model and observations. Unlike total ET, the error in the individual ET components (T, C, and E) are seasonally consistent. Continent wide, iCESM generally underestimates T and overestimates C and E (Supplemental Figures 1-3). This behavior is present across CMIP5 models and is attributed to numerous potential land surface models errors including errors in leaf area index (LAI), interception loss, root water uptake, light-use efficiency (LUE), and water-use efficiency (WUE) (Lian et al., 2018; Li et al., 2018). While all of these factors contribute to errors in the model simulated partitioning of ET, LUE is considered a potential major limitation for models given models often use LUE to estimate the gross primary productivity (GPP) of vegetation (Li et al., 2018). Across CMIP5 models, diffuse radiation is not explicitly represented in the land surface component (Lian et al., 2018), likely resulting in lower estimates of GPP (and photosynthetic activity) given the substantial impact diffuse radiation has on photosynthetic activity (Mercado et al., 2009). The Community Land Model (the land surface component of iCESM), is the only land surface model within CMIP5 that explicitly represents the diffuse-light dependence (Lian et al., 2018), potentially lowering the error in iCESM compared to other models. Despite the potential errors in iCESM, the error falls within the range of the Coupled Model Intercomparison Project Phase 6 (CMIP6) (Wang et al., 2021) and CMIP5 models (Mueller & Seneviratne, 2013). While we consider GLEAM observations as the “truth”, observational ET datasets are also prone to errors in ET estimations. GLEAM in particular overestimates the coupling strength between soil water content and ET (Qiu et al., 2019). Additionally, comparing the partitioning of ET into the three components between GLEAM, the Moderate Resolution Imaging Spectroradiometer evaporation product (PM-MOD), and the Priestley-Taylor Jet Propulsion Laboratory Model (PT-JPL) leads to drastically different partitioning with global T/ET values of 0.76, 0.24, and 0.56 (Miralles et al., 2016). Though errors are present in iCESM simulated ET, some of the error presented in Figure 3 and Supplemental Figures 1-3 likely stems from errors in the observational dataset.

https://doi.org/10.5194/hess-2021-284
Preprint. Discussion started: 11 June 2021

Hydrology and Earth System Sciences
Open Access
Discussions

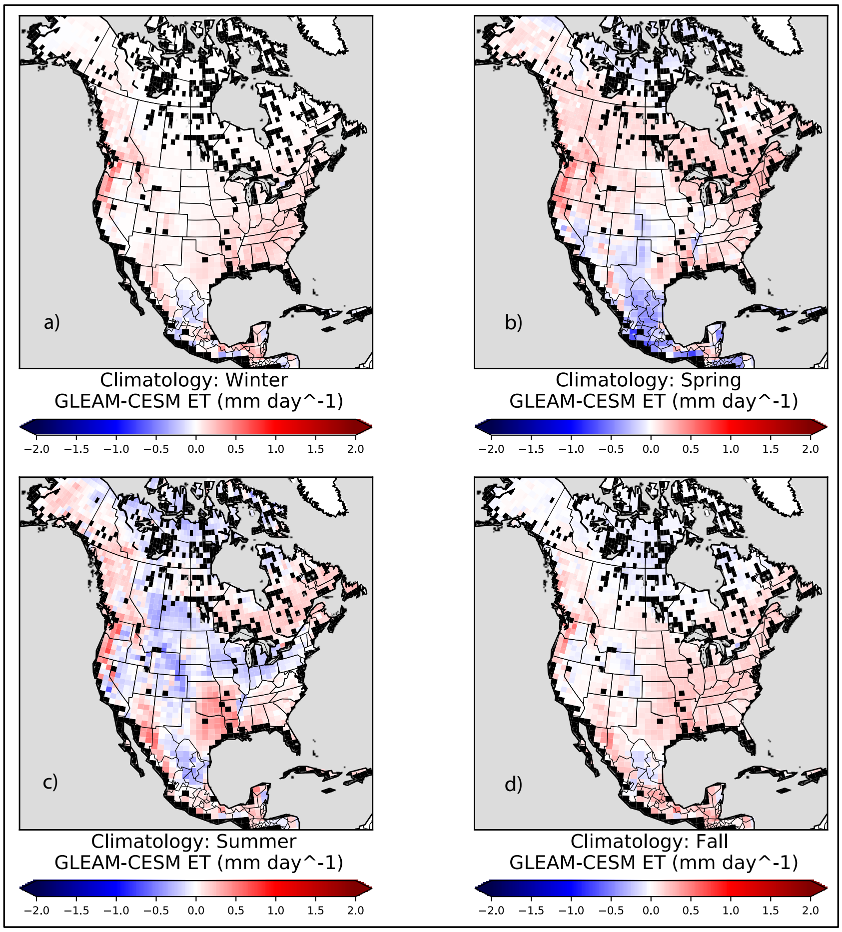

Figure 3. A comparison of the North American ET from iCESM and GLEAM for (a) Winter (DJF), (b) Spring (MAM), (c) Summer (JJA), and (d) Fall (SON). Note: black cells indicate missing observational data. Units are in mm day^-1.

3.3 Seasonal Land-Based Precipitation Signals

The average percent contribution of the global land surface to total precipitation over North America follows a seasonal cycle with the largest contributions in the summer and the smallest contributions in the winter. This is consistent with the reanalysis-based findings of van der Ent et al. (2010). During the winter months (DJF), the percent contribution of the land surface remains under 20% across the continent (Figure 4a). Meanwhile, the spring (MAM), summer (JJA), and fall (SON) seasons have maximum land surface contributions between 50-60%, 70-80%, and 40-50%, respectively (Figures 4b, 4c, & 4d). While the magnitude of land surface moisture contribution follows a seasonal cycle, the spatial patterns of maximum percent land moisture contribution remain fairly consistent across three of the four seasons. During the spring, summer, and fall, much of central Canada and the north-

https://doi.org/10.5194/hess-2021-284
Preprint. Discussion started: 11 June 2021

central US receive the greatest proportion of precipitation from the land surface while the western and southeastern coasts of the continent receive the smallest. The magnitude of the summer land surface contributions and spatial patterns presented here are fairly consistent with the findings of van der Ent et al. (2010), though we find the maximum contribution of the land surface extends further west. The spatial pattern of maximum land contribution during the winter season shifts to the south and east. The wintertime maximum contribution (15-20%) occurs in the central and eastern portions of the continent extending from southwestern Quebec, into the Great Lakes, the United States central plains, and into central/southern Mexico.

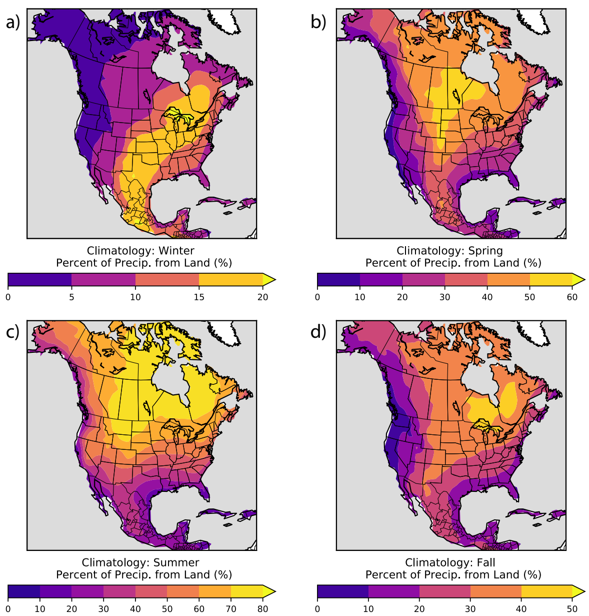

Figure 4. The percent contribution of land-based precipitation to total precipitation for (a) winter, (b) spring, (c) summer, and (d) fall. Note, the color bars are different for each panel. Units: %.

3.4 Seasonal Variations in Moisture Recycling

3.4.1 Winter Season Recycling

The land surface contributes less moisture for precipitation during the winter season than in any other season (Figure 4a). However, moisture recycling, defined as precipitation in a region that is sourced from ET within that region, still contributes between 2-4% of total precipitation across much of the southern United States, and over 4% in parts of Central America (Figure 5a, Supplemental Table 1a). Some areas near the Great Lakes also receive between 2-3% of their total precipitation from local moisture recycling, though this is likely from the Great Lakes themselves since lake evaporation is part of the E variable. While the contribution of local

https://doi.org/10.5194/hess-2021-284
Preprint. Discussion started: 11 June 2021

recycling to total precipitation is greatest in the south, local recycling comprises a considerable fraction of total winter land-based precipitation (total precipitation that is sourced only from the land surface) along the US west coast (Figure 6a, Supplemental Table 1b). Outside of the SMM region, the contribution of local recycling to total winter land-based precipitation is highest in the PNW and SWC regions. Approximately 34% of land-based precipitation in the PNW comes from local recycling, while 39% in the SWC comes from local recycling. Given that moisture recycling is highly dependent on the size and shape of the domain (Trenberth, 1999; van der Ent & Savenije, 2011; Dirmeyer & Brubaker, 2007), we also examine the normalized local recycling for each region. For these values, the recycling percentages from Figures 5a and 6a are scaled by the normalized land area of each region such that

$$\Lambda_i * \left|1 - \frac{\alpha_i}{\|\alpha_i\|}\right| \qquad (6)$$

where Λ is the percent recycling, α is the land area of each region, and $\|\alpha\|$ represents the Frobenius norm. This scaling ensures that regions with the largest land area are scaled down so the percent recycling is not solely a function of domain size. Both the PNW and SWC regions as well as the SMM region continue to have very high rates of local recycling when analyzing land-based precipitation only, even when considering the normalized values (Figure 6b, Supplemental Table 1c). Overall, results indicate that local moisture recycling is an important source of precipitation for much of Central America and the SCP region during the winter season.

https://doi.org/10.5194/hess-2021-284
Preprint. Discussion started: 11 June 2021

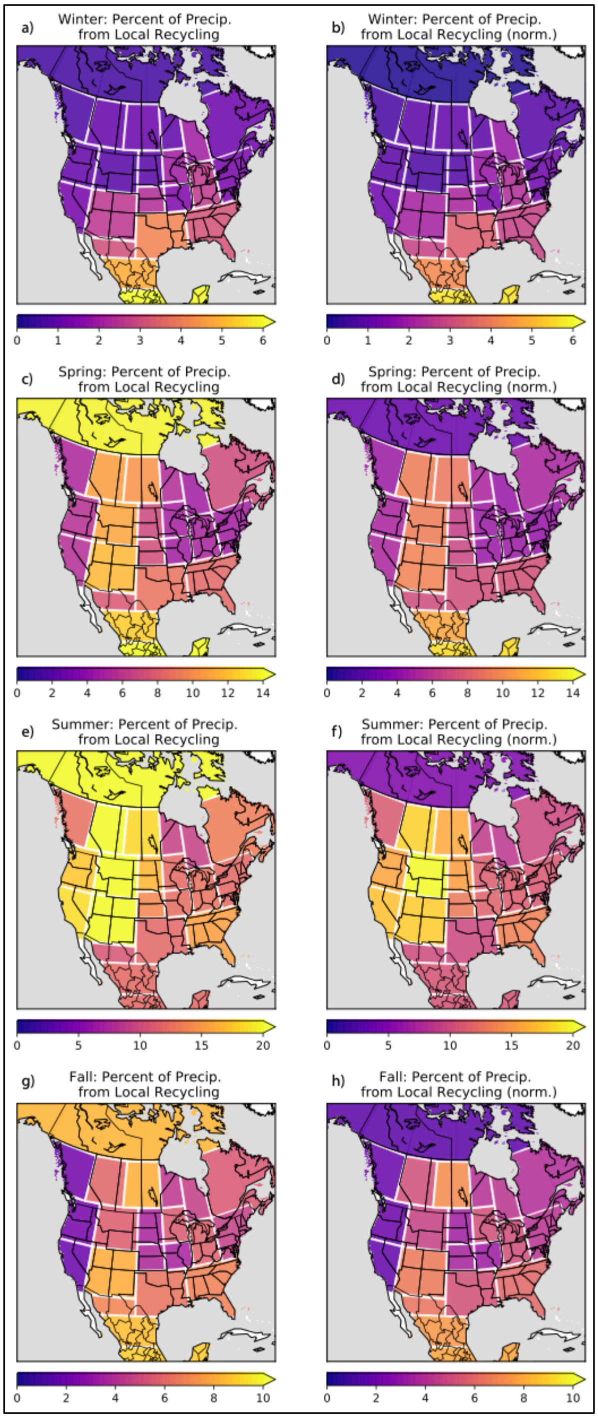

Figure 5. The percent contribution of local recycling to total precipitation during the (a) winter (DJF), (b) same as (a) but normalized by land area, (c) spring (MAM), (d) same as (c) but normalized by land area, (e) summer (JJA), (f) same as (e) but normalized by land area, (g) fall (SON), and (h) same as (g) but normalized by land area. Units: %.

https://doi.org/10.5194/hess-2021-284
Preprint. Discussion started: 11 June 2021

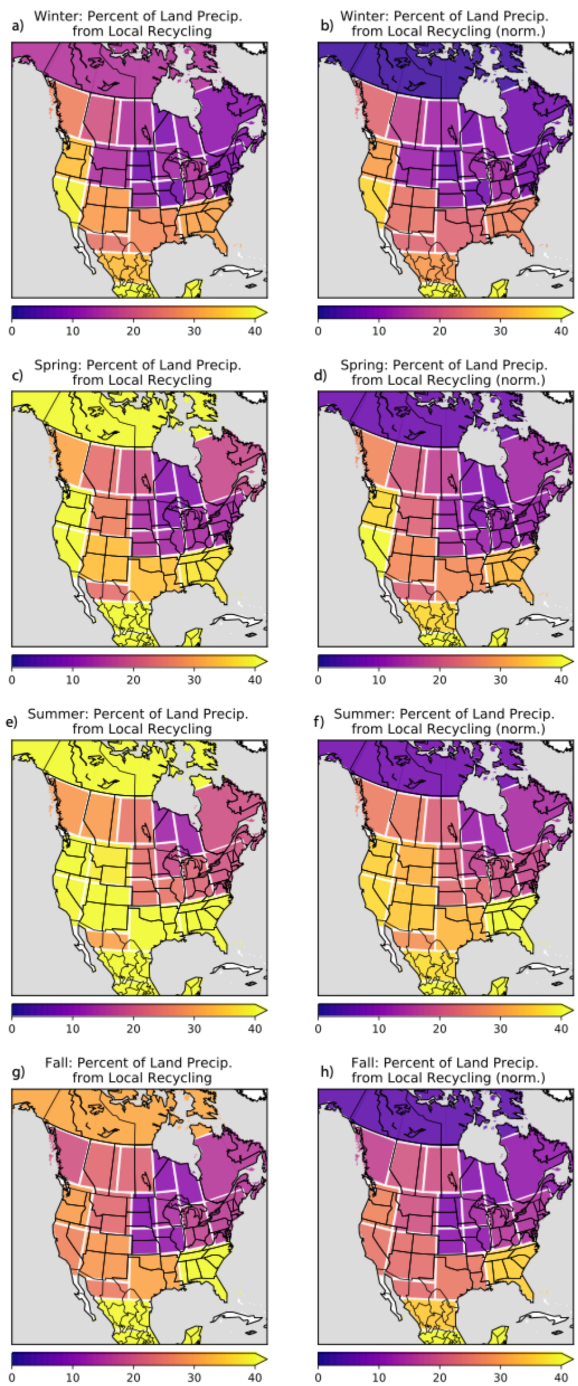

Figure 6. The percent contribution of local recycling to land-based precipitation during the (a) winter (DJF), (b) same as (a) but normalized by land area, (c) spring (MAM), (d) same as (c) but normalized by land area, (e) summer (JJA), (f) same as (e) but normalized by land area, (g) fall (SON), and (h) same as (g) but normalized by land area. Units: %.

https://doi.org/10.5194/hess-2021-284
Preprint. Discussion started: 11 June 2021

3.4.2 Spring Season Recycling

The maximum contribution of the land surface to total precipitation shifts to much of Canada and the central US during the spring season (Figure 4b). Along with the northwestward shift in land surface contribution, the role of local moisture recycling increases during the season as well (Figure 5c, Supplemental Table 2a). All of the land regions in the US Intermountain West and the Canadian Prairies receive between 10% and 12% of their total springtime precipitation from local moisture recycling. Local recycling contribution also increases dramatically in the NCA region going from 0.6% in the winter to 14% in the spring. Local recycling remains important in Central America with precipitation contributions between 12-15%. While the normalization dramatically decreases the recycling for the large NCA region, the US Intermountain West, Canadian Prairies, and Central America recycling values remain high in comparison to the rest of the continent indicating the recycling values are not solely a function of the size of these regions (Figure 5d, Supplemental Table 2c).

Similar to the winter season, local recycling remains a major source of land-based precipitation for the west coast of the US during the spring (Figure 7a, Supplemental Table 2b). Additionally, local recycling is an important source of moisture for land-based precipitation in the NCA, CMM, and SMM regions. For these top 5 regions (PNW, SWC, NCA, CMM, & SMM), local recycling contributes 41, 48, 40, 42, and 64% respectively of the land-based precipitation within those regions. However, Figure 7b suggests that the high percent contribution in NCA is likely the result of a large study region. Since the NCA region is defined from the west coast of Alaska to the east coast of Canada, any land surface moisture that evaporates in the west and precipitates in the east is considered "local" recycling. In contrast, the other four regions continue to have high normalized recycling values (Figure 7b, Supplemental Table 2d), further emphasizing the importance of local recycling for land-based precipitation in those regions.

3.4.3 Summer Season Recycling

During the summer, the land surface is a major source of moisture for much of the North American continent (Figure 4c). The contribution of local moisture recycling to total precipitation also increases for the entire continent during this season (Figure 5e, Supplemental Table 3a). The highest contributions of local recycling occur in the western US with 27% of UPR and 22% of SWW precipitation coming from recycled moisture. Across the central and southern US, local recycling accounts for 12% to 17% of total summertime precipitation. Recycled moisture is also an important moisture source for WIP, EIP, and NCA contributing 21, 18, and 27% of precipitation respectively. Even after normalizing the recycling values, the western US and Canadian Prairies continue to have the highest recycling percentages in North America (Figure 5f, Supplemental Table 3c) Unlike the winter and spring seasons, local recycling contributes over 39% of land-based precipitation for all of the southern and western US, Central America (except NMM), and NCA (Figure 8a, Supplemental Table 3b). These high

https://doi.org/10.5194/hess-2021-284
Preprint. Discussion started: 11 June 2021

recycling values remain, particularly in the SSE region, even after scaling for domain size (Figure 8b, Supplemental Table 3d). For these regions, local land surface moisture is a critical moisture supply during the summer season. However, for much of northeastern North America, the contribution of local recycling to both land-based precipitation and total precipitation is much lower. Given the high (>50%) contribution of the land surface to precipitation across this portion of the continent (Figure 4c), this suggests moisture transport from upwind land regions is a significant source of summertime precipitation.

3.4.4 Fall Season Recycling

The spatial pattern of land-surface contribution to precipitation is very similar between the spring and fall seasons, though the magnitude of the contribution is slightly lower in the fall (Figures 4b, 4d). Similar to the land-surface contribution, the contribution of local recycling to precipitation is also spatially similar between the fall and the spring (Figures 5c, 5g, Supplemental Tables 2a, 4a). Over 8% of precipitation comes from local recycling in NCA, EIP, SWW, CMM, and SMM, with the highest contribution of 9% in SMM. Other than the NCA region, the scaled recycling values indicate the same regions rely more on local recycling for precipitation than the rest of the continent (Figure 5h, Supplemental Table 4c). Consistent with the summer, the highest percentages of land-based precipitation from local recycling occur in the southern and western US and Central America (Figure 9a, Supplemental Table 4b). Although the same regions have the highest recycling percentages, the magnitude of those percentages drop in all of the western and southern US regions by over 9% except for the SSE region (5% decrease). There are also large decreases (≥13%) in the local recycling percentage of land-based precipitation in most of the central US (ICP, INP, & RMW). However, these regions still receive approximately 30-40% of their fall precipitation from land surface moisture (Figure 4d), so moisture transport into the central US proves to be an essential source of moisture for fall precipitation.

3.5 Divergence and Convergence of North American Land Moisture

Land surface evaporation that does not precipitate locally is exported out of its evaporative source region and is available for precipitation elsewhere. Equation (5) contains two key components of moisture transport: the divergence of locally evaporated moisture and the convergence of remotely evaporated moisture (Singh et al., 2016). Our framework modifies these two terms such that $-\ddot{\mathbf{T}}\vec{\ddot{E}}$ represents the divergence of land-sourced moisture to other North American land regions, and $\mathbf{F}\ddot{\mathbf{T}}\vec{\ddot{E}}$ represents the convergence of remotely evaporated North American land-sourced moisture. This formulation provides a mechanism to examine the primary sources and sinks of land-based precipitation within the context of the North American continent.

https://doi.org/10.5194/hess-2021-284
Preprint. Discussion started: 11 June 2021

Hydrology and Earth System Sciences
Open Access
Discussions

3.5.1 Winter Transport of ET

The predicted precipitation using Equation (5) captures both the spatial variability and the magnitude of CESM-simulated North American land-based precipitation (Supplemental Figures 1-2). The spatial patterns of $-\ddot{\mathbf{T}}\vec{\ddot{E}}$ (from hereon called the divergence term) and $\mathbf{F}\ddot{\mathbf{T}}\vec{\ddot{E}}$ (from hereon called the convergence term) indicate seasonal shifts in the key land moisture source and sink regions (Figure 10). During the winter season, the magnitude of the divergence term is highest in the southern US and Central America, aligning closely with the evaporation fields (Figures 10a and 10b). Though higher evaporation totals potentially allow for higher amounts of moisture divergence, our framework developed in Section 2.2 only considers moisture divergence that later converges within North America. Differences between the evaporation fields and the divergence fields are attributed either to high amounts of internal moisture recycling or to atmospheric circulation features that may export evaporation from some land regions out of the North American domain. The evaporation is highest in the SMM region, but the SMM divergence term is relatively equivalent to that of the CMM region. Given the high amounts of local recycling during the winter in the SMM region (Figures 5a-b, 6a-b), local recycling likely accounts for the lower value of divergence. Despite the concentration of high divergence values in the southern portions of the continent, the magnitude of the convergence term during the winter is highest along the eastern coast of the continent extending from the SCP region up to ALC. This suggests that atmospheric circulation features transport supplies of terrestrial ET from the south to the north for precipitation.

3.5.2 Spring Transport of ET

The divergence field shifts north from the winter to the spring season (Figure 10e). Both the US west coast and the US central/southern plains exhibit high divergence term magnitudes during the spring season relative to the rest of the continent. The US central/southern plains also exhibit high levels of evaporation allowing for their high divergence values (Figure 10d). Both the SSE and SMM regions also experience high levels of evaporation, but their divergence terms are relatively weaker. Consistent with the winter season, local recycling in the SMM region contributes a considerable amount to total precipitation (Figures 5c-d, 7a-b) likely reducing the amount of evaporation available for export. However, local recycling in the SSE region is of a similar magnitude as the SCP region indicating atmospheric circulation likely exports SSE moisture off the continent to the Atlantic Ocean. Similar to the divergence field, the magnitude of the convergence field increases across much of the northern US and southern Canada from the winter to the spring season (Figure 10f). The spatial variation of these two terms during the spring season indicates that both the US west coast and central plains are important sources of land-based moisture for much of the continent.

3.5.3 Summer Transport of ET

The maximum divergence shifts to the north again from the spring to the summer season resulting in the highest divergence values across the US Northwest, US central/northern plains, and the Canadian Prairies (Figure 10h). The corresponding evaporation field closely aligns with the divergence values except in the OHV, SSE, and NEE regions (Figure 10g). During the summer season, the SSE receives 46% of land-based precipitation from internal local recycling (Table 3b), far exceeding the US central/northern plains regions or the Canadian Prairies (Figures 8a-b), and likely reducing the moisture available for export. While the OHV and NEE both have local recycling of a similar magnitude to the central/northern US plains (Figures 5e-f, 8a-b), given their proximity to the east coast and prevailing atmospheric circulation features, they likely export a large fraction of their evaporation out to the Atlantic, resulting in low divergence values. The convergence field exhibits similar behavior to the divergence field with higher values across the northern US and Canada and lower values across the southern US and Central America (Figure 10i). These spatial patterns indicate many of the agricultural hotspots in the central US and the Canadian Prairies are key source regions of land-sourced moisture for the northern half of North America.

3.5.4 Fall Transport of ET

During the fall season, the divergence field is more spatially diffuse across the continent than in the summer season (Figure 7k). The highest magnitudes of divergence are present across much of the southern and eastern US, largely consistent with the evaporation field (Figure 7j). While the evaporation and divergence fields are consistent for most regions, the OHV, NEE, CMM, and SMM regions all have higher evaporation fields than their divergence fields suggest. Consistent with the summer season, the OHV and the NEE regions likely transport their moisture out of the North American domain given the low amounts of internal recycling (Figures 5g-h, 9a-b). However, both CMM and SMM rely on internal local recycling for large fractions of their precipitation (Figures 5g-h, 9a-b) likely lowering the available moisture for export. Unlike the divergence field, the convergence field is more concentrated to the northeast, aligning closely with the maximum percent contribution of the land surface to total precipitation (Figure 4d). Though the SSE and NMW regions exhibit the highest magnitudes of the divergence term, the spatial diffusivity of the divergence term in the fall season in comparison to the other seasons suggests the high convergence in the northeast is sourced from a wide range of regions continent-wide.

https://doi.org/10.5194/hess-2021-284
Preprint. Discussion started: 11 June 2021

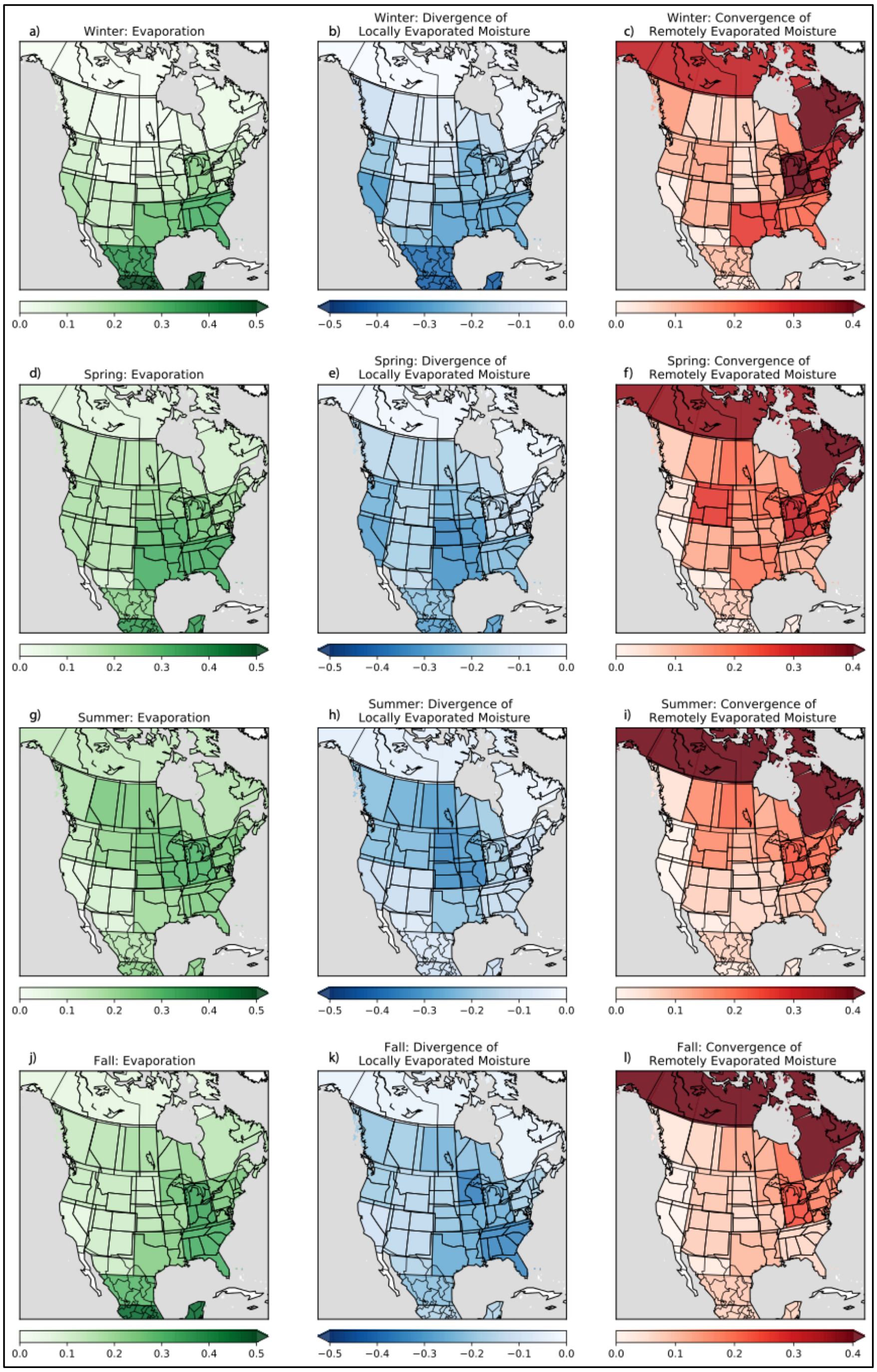

Figure 7. (a) Winter ET, (b) winter divergence of locally evaporated ET, (c) winter convergence of remotely evaporated ET, (d) spring ET, (e) spring divergence of locally evaporated ET, (f) spring convergence of remotely evaporated ET, (g) Summer ET, (h) summer divergence of locally evaporated ET, (i) summer convergence of remotely evaporated ET, (j) Fall ET, (k) fall divergence of locally evaporated ET, and (l) fall convergence of remotely evaporated ET. All units are normalized units of length per m^-1.

https://doi.org/10.5194/hess-2021-284
Preprint. Discussion started: 11 June 2021

3.6 Variations in Precipitation from each Evapotranspiration Component

Using the expanded water tracing capabilities of CESM, we are able to split the land-based precipitation into precipitation from T, C, and E moisture individually. This allows us to directly investigate the varying contributions of each ET component to precipitation fields, moisture recycling, and moisture transport.

3.6.1 Annual T/E/C Contributions

The annual climatology of the percent contribution of the land surface to total precipitation is spatially consistent with the spring (Figure 4b) and fall (Figure 4d) seasons (Figure 8a). The maximum land surface contribution of 50-60% is confined largely to central Canada and the north-central US. Consistent with all of the seasonal values (Figure 4), the annual climatology also indicates the western and southeastern coasts of North America receive the lowest percent contributions from the land surface. On an annual basis, T moisture (moisture from transpiration) comprises 45-50% of the land-based precipitation across a large swath of the continent from Alaska, northwestern Canada, the north-central US, and much of the east coast of the US and Canada (Figure 8b). The lowest contributions of T (25-30%) occur in the western US and northern Mexico where T is limited due to a lack of vegetation and the arid environment. The proportion of land-based precipitation originating from C moisture (moisture evaporated directly from plant surfaces) ranges from 15-25% across much of the continent (Figure 8c). Only Alaska, northwestern Canada, portions of the southeastern US, and Central America receive 25% of more of their land-based precipitation from C moisture. These same areas receive the lowest contribution from E moisture (moisture evaporated directly from ground and lake surfaces), with totals ranging from 15-25% (Figure 8d). In contrast, the highest contributions (45%) from E moisture occur in the western/southwestern US and portions of far northern Canada. The Great Lakes also show high E contributions, though this is likely a result of lake evaporation.

https://doi.org/10.5194/hess-2021-284
Preprint. Discussion started: 11 June 2021

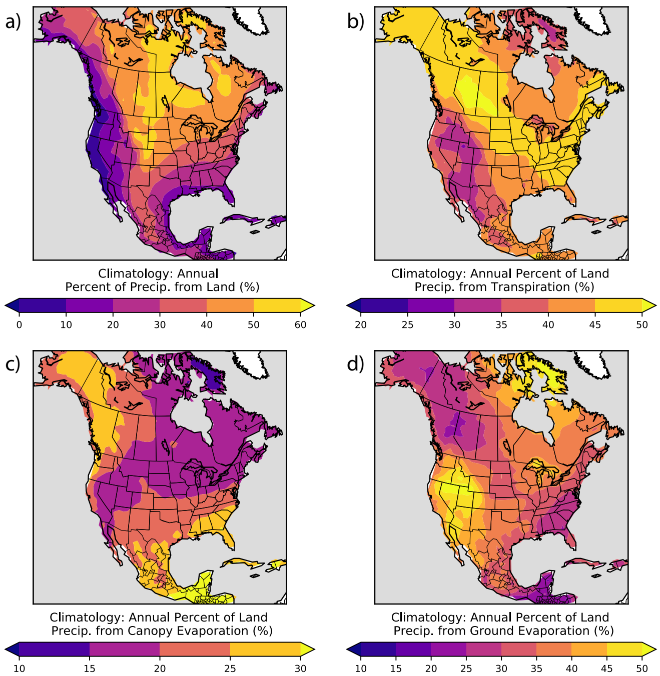

Figure 8. (a) The annual percent contribution of land-based precipitation to total precipitation, (b) the percent of land-based precipitation originating from T, (c) the percent of land-based precipitation originating from C, and (d) the percent of land-based precipitation originating from E. Units: %.

3.6.2 Winter Season T/E/C Contributions

During the winter season, E moisture is the most prominent source of land-based precipitation for most of the continent, contributing between 40-60% of the total precipitation originating from the land surface (Figure 9d). The lowest contributions of E are seen in the Canadian prairies (30-40%), southeastern United States (30-40%), and much of Central America (10-40%). The fraction of winter precipitation sourced from C moisture is also fairly uniform across much of the continent, comprising 10-30% of the land-based precipitation over a wide area (Figure 9c). The maximum contribution of C (30-50%) occurs across western Canada, specifically within the prairies. Unlike E and C, there is a clear gradient in the contribution of T moisture to total land-based precipitation (Figure 9b). The contribution of T has a minimum across central Canada (10-20%) and increases towards the coasts and towards the south. T contributes most to winter land-based precipitation in parts of the southeastern US and Central America, with fractional contributions between 40% and 50%.

https://doi.org/10.5194/hess-2021-284
Preprint. Discussion started: 11 June 2021

Hydrology and Earth System Sciences
Open Access
Discussions

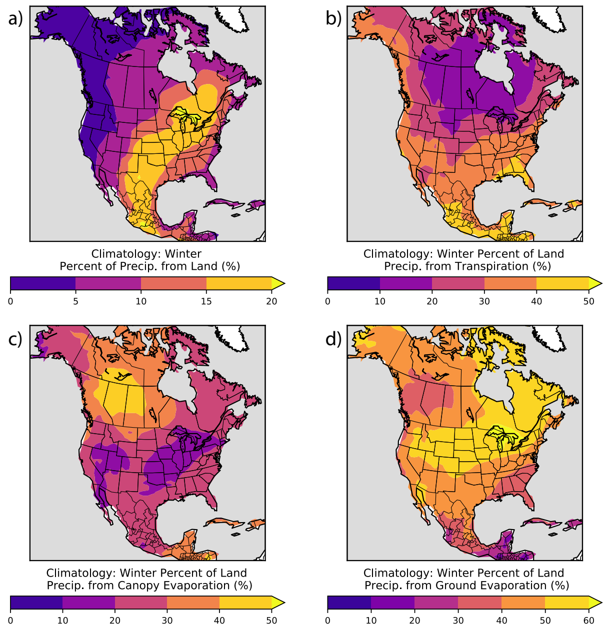

Figure 9. (a) The percent contribution of land-based precipitation to total precipitation during the winter (DJF), (b) the percent of land-based precipitation originating from T, (c) the percent of land-based precipitation originating from C, and (d) the percent of land-based precipitation originating from E. Units: %.

3.6.3 Spring Season T/E/C Contributions

In the spring, the role of T increases across the continent as leaf out occurs and vegetation extent increases. T contributes 40-50% of the land-based precipitation for all of the central and eastern United States and for Central America (Figure 10b). Across much of Canada and the western US, the contribution of T moisture is lower at 20%-40%. Moisture contribution from C is fairly uniform during the spring season (Figure 10c). Most of the continent receives 10-20% of springtime, land-based precipitation from C. The contribution of C increases to 20-30% in the southeastern portions of the continent and along much of the west coast. As the proportion of T:ET increases from winter to spring, the contribution of E declines. In contrast with winter E, a gradient of increasing percent contribution from the SE to the NW develops across the continent in the spring (Figure 10d). The contribution of E has a minimum in the southeast (0-20%) and increases gradually towards the north and west, with the maximum contribution of 50-70% occurring across much of northern Canada and Alaska.

https://doi.org/10.5194/hess-2021-284
Preprint. Discussion started: 11 June 2021

Hydrology and Earth System Sciences
Open Access
Discussions

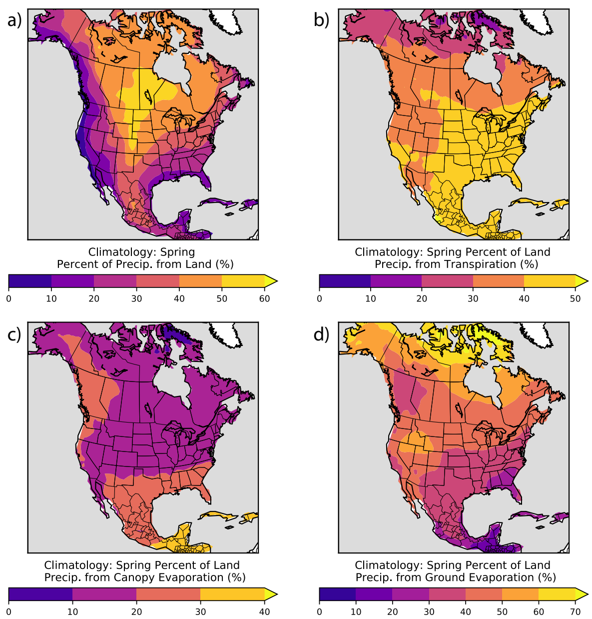

Figure 10. (a) The percent contribution of land-based precipitation to total precipitation during the spring (MAM), (b) the percent of land-based precipitation originating from T, (c) the percent of land-based precipitation originating from C, and (d) the percent of land-based precipitation originating from E. Units: %.

3.6.4 Summer Season T/E/C Contributions

T is the dominant source of land-based precipitation for most of North America during the summer season. Outside the southwest US and western Mexico, T contributes over 40% of the total land-based precipitation for the rest of the continent and over 50% for much of Canada and the northern half of the United States (Figure 11b). Though the role of E moisture declines further in the summer for much of the continent as vegetation extent reaches a maximum, the summertime patterns of E are fairly consistent with and reversed from those of T (Figure 11d). Much of Canada and the northeastern half of the US receives 10-30% of land-based precipitation from E. Most of the US southwest and far northeast Canada receive higher percentages (40-60%) from E. The spatial patterns of C-based precipitation do not resemble the patterns of T or E (Figure 11c). C is responsible for 20-30% of the land-based precipitation across western Canada, Alaska, and nearly all of the United States and Mexico. Slightly lower percent contributions (10-20%) are present across Eastern Canada and portions of the western US.

https://doi.org/10.5194/hess-2021-284
Preprint. Discussion started: 11 June 2021

Hydrology and Earth System Sciences
Discussions

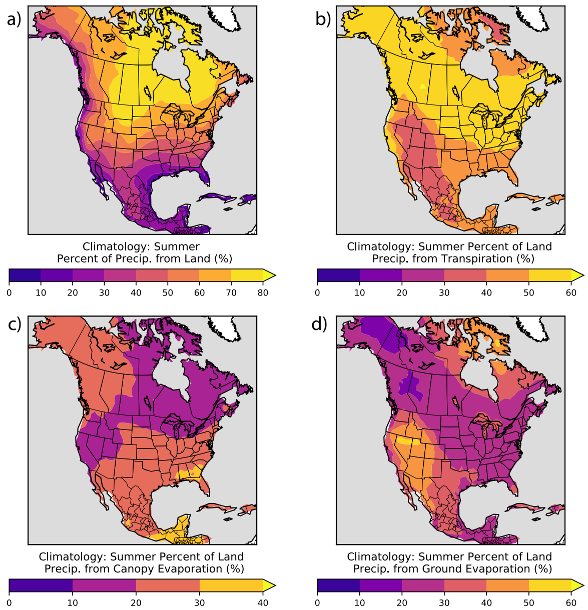

Figure 11. (a) The percent contribution of land-based precipitation to total precipitation during the summer (JJA), (b) the percent of land-based precipitation originating from T, (c) the percent of land-based precipitation originating from C, and (d) the percent of land-based precipitation originating from E. Units: %.

3.6.5 Fall Season T/E/C Contributions

During the fall season, the role of T begins to decline as plant senescence begins and vegetation extent declines. Most of North America receives 30-40% of land-based precipitation from T during this season (Figure 12b). Areas along the east coast of the US, Canadian west coast, Alaska, and Central America receive slightly higher amounts from T (40-50%), while portions of the interior western US and the Great Lakes receive slightly lower amounts (20-30%). C is uniform across the continent (20-30%) except for western Canada/Alaska and Central America (30-40%), and a few small areas in the US southwest and Great Lakes regions (10-20%) (Figure 12c). A large portion of the continent from the US southwest to northeastern Canada receives 40-50% of land-based precipitation from E (Figure 12d). The contribution from E declines along the east coast of the US, Central America, Western Canada, and Alaska to 20-40%. The only areas to exceed 50% E contribution are around the Great Lakes and a small region in the semi-arid western US, largely overlapping the area with the lowest T contributions.

https://doi.org/10.5194/hess-2021-284
Preprint. Discussion started: 11 June 2021

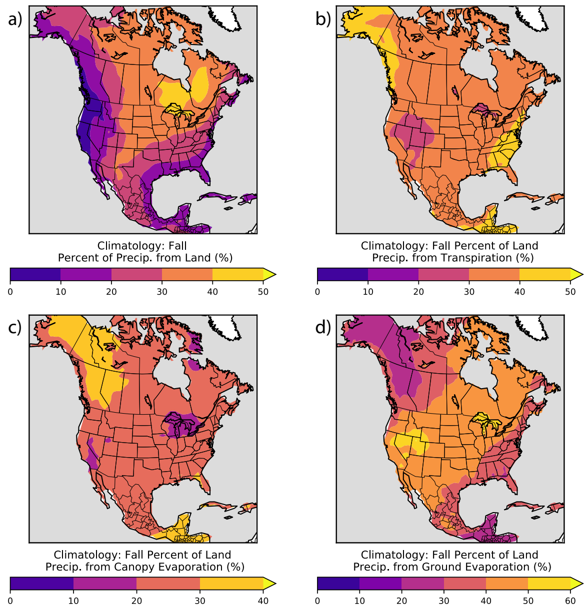

Figure 12. (a) The percent contribution of land-based precipitation to total precipitation during the fall (SON), (b) the percent of land-based precipitation originating from T, (c) the percent of land-based precipitation originating from C, and (d) the percent of land-based precipitation originating from E. Units: %.

3.7 Decomposing Moisture Recycling and Transport into T/E/C Components

The dominant ET component for recycling is highly dependent on the season. During the winter season when T contribution is low, the combination of E and C dominate moisture recycling across the continent (Figure 13a, Supplemental Table 5). C is the main source of recycled moisture across most of southern Canada during this season, while E dominates across much of the US. The role of T in local recycling increases for every region from winter to spring (Figure 13b, Supplemental Table 6), though the combination of E and C is still responsible for the majority of recycled moisture. However, during the summer season, T becomes the largest contributor to recycled moisture for much of the north and eastern portions of the continent (Figure 13c, Supplemental Table 7). T comprises over 40% of local recycling for all regions except the west coast of the US, the southwest US, the SCP, and Central America. For many of these regions, E remains the largest source of recycled moisture contributing over 41% for the PNW, SWC, SWW, NMM, and CMM regions. During the fall season, E and C dominate local recycling (Figure 13d, Supplemental Table 8). T only contributes more than 40% of the local recycling in the NEE and SSE regions.

Similar to the recycled moisture, the composition of transported land moisture varies by the season. In the winter, E is the primary land moisture source for most of the continent (Figure 14a, Supplemental Table 9). In the southern US and Central America, there is a fairly even split between transported E and T moisture, though E still exceeds T in all regions except for SWC,

https://doi.org/10.5194/hess-2021-284
Preprint. Discussion started: 11 June 2021

CMM, and SMM. Transported T moisture increases in the spring contributing over 35% of transported land moisture in all regions (Figure 14b, Supplemental Table 10). Even with the increased transport of T, E still remains the top source of transported land moisture across all of Canada and the western US except for SWW. During the summer season, T contributes over 41% of transported moisture and is the top source of transported moisture for all regions except for the SWC where E remains the dominant source of transported moisture (Figure 14c, Supplemental Table 11). Additionally, T accounts for 50% or greater of transported moisture across the continent except for SWC, SWW, UPR, SCP, ICP, NMM, CMM, and SMM. The role of transported T moisture decreases again in the fall season, only contributing 40% or more in the PNW, NCA, PFC, and SMM regions (Figure 14d, Supplemental Table 12).

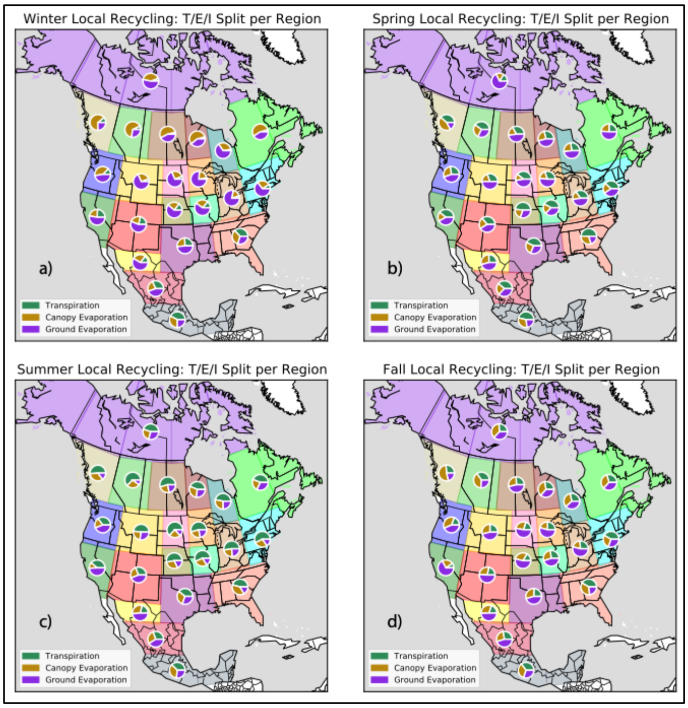

Figure 13. (a) The percent contribution of T, C, and E to total local precipitation recycling during the winter (DJF), (b) the same as (a) for the spring (MAM), (c) the same as (a) for the summer (JJA), and (d) the same as (a) for the fall (SON)

https://doi.org/10.5194/hess-2021-284
Preprint. Discussion started: 11 June 2021

Hydrology and Earth System Sciences
Open Access
Discussions

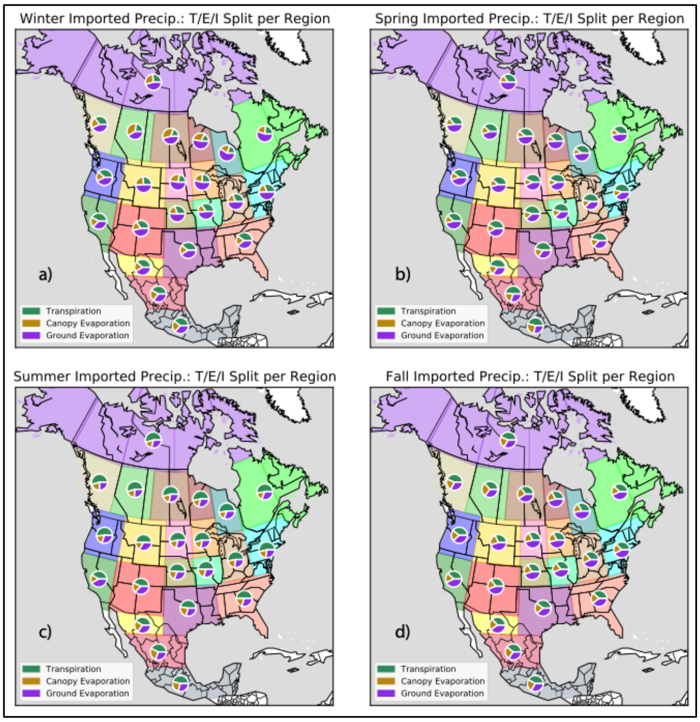

Figure 14. (a) The percent contribution of T, C, and E to total, non-recycled, land-based precipitation during the winter (DJF), (b) the same as (a) for the spring (MAM), (c) the same as (a) for the summer (JJA), and (d) the same as (a) for the fall (SON)

3.8 Divergence and Convergence of the ET Components

The same framework developed in Section 2.2 used to examine the divergence and convergence of total land surface ET in Section 3.5 can be used to examine the behavior of the individual ET components. Equation (5) is modified for each individual flux such that

$$\vec{\ddot{P}}_T = \vec{\ddot{E}}_T - (\mathbf{I} - \mathbf{F}_T)\ddot{\mathbf{T}}_T\vec{\ddot{E}}_T \qquad (6)$$

$$\vec{\ddot{P}}_C = \vec{\ddot{E}}_C - (\mathbf{I} - \mathbf{F}_C)\ddot{\mathbf{T}}_C\vec{\ddot{E}}_C \qquad (7)$$

$$\vec{\ddot{P}}_E = \vec{\ddot{E}}_E - (\mathbf{I} - \mathbf{F}_E)\ddot{\mathbf{T}}_E\vec{\ddot{E}}_E \qquad (8)$$

where P, E, **F**, and **T** are defined the same as in Section 2.2 except now they apply only to T in Equation (6), C in Equation (7), and E in Equation (8). Consistent with Section 3.5, $-\ddot{\mathbf{T}}_T\vec{\ddot{E}}_T$ represents the divergence of T-sourced moisture (from here on referred to as the T-divergence term), $-\ddot{\mathbf{T}}_C\vec{\ddot{E}}_C$ represents the divergence of C-sourced moisture (from here on referred to as the

https://doi.org/10.5194/hess-2021-284
Preprint. Discussion started: 11 June 2021

C-divergence term), $-\ddot{\mathbf{T}}_E\vec{\ddot{E}}_E$ represents the divergence of E-sourced moisture (from here on referred to as the G-divergence term), $\ddot{\mathbf{F}}_T\ddot{\mathbf{T}}_T\vec{\ddot{E}}_T$ represents the convergence of T-sourced moisture (from here on referred to as the T-convergence term), $\ddot{\mathbf{F}}_C\ddot{\mathbf{T}}_C\vec{\ddot{E}}_C$ represents the convergence of C-sourced moisture (from here on referred to as the C-convergence term), and $\ddot{\mathbf{F}}_E\ddot{\mathbf{T}}_E\vec{\ddot{E}}_E$ represents the convergence of E-sourced moisture (from here on referred to as the E-convergence term). These terms allow for the direct investigation into the varying behavior of individual moisture flux sources rather than assuming all the components behave in a similar manner as total ET.

3.8.1 Winter Transport of T, C, and E

The predicted precipitation for each moisture flux using Equations (6)-(8) captures both the spatial patterns and the magnitude of CESM-simulated North American precipitation sourced from T, C, and E individually (Supplemental Figures 3-8). The winter divergence fields reveal disparate behavior for each moisture flux source (Figures 15-17b). T-divergence is confined primarily to the southern regions of the continent where vegetation remains active during the winter months and T is the highest (Figure 15a). Unlike T-divergence, both C and E divergence extend from Central America to southern Canada. Consistent with the C field (Figure 16a), the magnitude of winter C-divergence is highest in the PNW, PFC, and SMM regions and is moderately high across much of the central and southeastern US. The magnitude of E-divergence is also high in these regions, though the maximum magnitude of E-divergence occurs in the Great Lakes region. While the E field closely aligns with E-divergence, the E in both the SMM and OHV regions exceeds their respective divergence values (Figures 17a-b). As noted in Section 3.5, using our framework, differences between the evaporation and divergence fields can arise from high amounts of internal recycling or from moisture export out of the North American domain. Though the percent of local recycling from E is low in SMM (Figure 13a), total local recycling is high (Figures 6a-b). Conversely, local recycling in the OHV region is relatively low (Figures 6a-b), but the contribution of E to local recycling is very high (Figure 13a). In both cases, recycling and their proximity to the oceanic regions (leading to an increased amount of moisture export leaving the North American domain) likely reduces their overall divergence values. Despite varying behavior in the divergence fields, all three fluxes have the highest convergence magnitudes along the eastern coast of North America during the winter season. However, maximum C-convergence and E-convergence is confined further northeast than T-convergence (Figures 15-17c). This is likely a result of higher T-divergence in Central America converging in the southern and southeastern US allowing maximum T-convergence values to extend further south than E or C-convergence. This behavior is consistent with high percent contributions of T to total imported precipitation during the winter season in the SCP and SSE regions (Figure 14a).

https://doi.org/10.5194/hess-2021-284
Preprint. Discussion started: 11 June 2021

3.8.2 Spring Transport of T, C, and E

As vegetation becomes more active across the continent during the spring season, the T field increases (Figure 15d), and the resulting T-divergence shifts north from the winter season (Figure 15e). The southern US plains, southeastern US, and SMM region have high amounts of T flux and T-divergence. Though the SSE and SMM regions have the largest T flux during the spring season, the T-divergence is largest in the central and southern plains indicating that the SSE and SMM regions either recycle the excess T moisture or it is exported out of the North American domain. Local recycling is high in both regions, particularly in SMM (Figures 7a-b), and T is the largest contributor to recycled precipitation in both regions (Figure 13b). As with the winter season E, the combination of local recycling and proximity to the coasts likely reduce the T moisture divergence from these regions. Unlike the T-divergence, C-divergence remains relatively unchanged between the winter and spring seasons (Figure 16e). Both the highest C flux and the highest C-divergence remains in the PNW, PFC, and SMM regions, though C-divergence increases across the central/southern plains in the US during the spring. The spring E-divergence field is moderately high across the entire western half of the US with the highest magnitudes along the US west coast and in the central/northern plains. The C and E evaporation fields are fairly consistent with their respective divergence fields during the spring season, though C is higher in the SSE and E is higher in the OHV than their divergence values (Figures 16-17d). Though E contributes more to internal recycling in the OHV region than the other two moisture fluxes (Figure 13b), local recycling remains low during the spring season (Figures 7a-b). The inconsistencies between the evaporation and divergence fields indicate both regions export a considerable amount of moisture out of North America. Despite differences between the divergence fields, the spring convergence fields are very similar across the three fluxes (Figures 15-17f). The northern half of North America (with the exception of the immediate west coast) generally has the highest values of convergence for all three fluxes. Additionally, the SCP region has a high convergence magnitude for each flux, likely the result of divergence fields from Central America.

3.8.3 Summer Transport of T, C, and E

The convergence magnitudes for all three fluxes remain high across the northern half of the continent during the summer while both the western and southern portions of the continent have very low convergence magnitudes (Figures 15-17i). Both the T and T-divergence maximums also shift north from the central/southern US plains in the spring to the central/northern US plains and the Canadian Prairies during the summer (Figures 15g-h). Given that the model configuration used in this study includes both crop management and irrigation, the northward seasonal shift in maximum T-divergence could be related to agricultural harvesting and irrigation patterns, though this is not addressed directly in this study. The T evaporation field is consistent with the T-divergence field across the continent except for the OHV and NEE

https://doi.org/10.5194/hess-2021-284
Preprint. Discussion started: 11 June 2021

regions where the amount of T far exceeds the divergence (Figures 15g-h). Although T is the dominant moisture source for local recycling in both regions (Figure 13c), recycling is relatively low (Figures 8a-b). The differences between T and T-divergence in the OHV and NEE regions are attributed to atmospheric circulation exporting excess evaporation into the Atlantic Basin. Similar to T-divergence, summer C-divergence is high across the Canadian Prairies and central/northern plains, and is also high in the SCP, SSE, and SMM regions (Figure 16h). Despite higher amounts of C in the SSE and SMM regions, the C-divergence is highest in western Canada and the central US indicating more C-moisture exported from these regions converges and precipitates within North America. Additionally, summer local recycling is very high in both the SSE and SMM regions (Figures 8a-b), and C moisture comprises over 35% of the recycled moisture in each region (Figure 13c, Supplemental Table 7b). This implies that both regions export C moisture off the coast of North America and recycle large quantities of C moisture, reducing their C-divergence. The magnitudes of E-divergence are highest across much of central/western US and southern Mexico, and E-divergence is generally higher (lower) in the regions where C-divergence is lower (higher) (Figure 17h). This behavior is consistent with studies showing that as interception increases, soil moisture (and the resulting soil evaporation) decreases (Lawrence et al., 2007). The maximum summer E-divergence occurs in the PNW region, likely leading to the high E-convergence values in the WIP, EIP, and UPR regions (Figure 17i). The E fields for several regions are inconsistent with the E-divergence during the summer season (Figures 17g-h). The OHV, NCA, ALC, CMM, and SMM regions all have higher E magnitudes than their respective E-divergence fields suggest. Each of these regions borders at least one ocean (NCA, CMM, and SMM border two), so moisture export loss to the oceans is likely. Additionally, summer recycling is very high in the CMM, SMM, and NCA regions, further reducing the amount of E available for export (Figures 8a-b). The E and E-divergence fields are also inconsistent between the PNW and UPR regions. Both regions have relatively equal E magnitudes, but the PNW E-divergence magnitude is much greater than the UPR E-divergence (Figures 17g-h). This difference is largely attributed to the increased land area available for PNW E moisture to precipitate given a traditional westerly atmospheric flow across North America. This also allows PNW moisture to precipitate as a result of topography in the UPR region, while much of the UPR E moisture may evaporate east of the model's resolved topography, limiting the orographically-induced precipitation.

3.8.4 Fall Transport of T, C, and E

During the fall season, the highest convergence values for all of the fluxes cluster in the far northeastern portions of North America (Figures 15-17l). T-convergence in particular stays relatively confined to the northeast, while C-convergence has some moderately high values further west in the WIP, EIP, and UPR regions. As vegetation begins to die off in the fall season, both T and T-divergence maximums shift to the south and southeast (Figures 15j-k). The highest values of T occur in the SSE and SMM regions, but only the SSE has a very high magnitude of

https://doi.org/10.5194/hess-2021-284
Preprint. Discussion started: 11 June 2021

T-divergence. While both the SMM and SSE regions recycle a lot of land-sourced moisture in the fall season (Figures 9a-b), the recycling in the SMM region exceeds that of the SSE by approximately 8% (Supplemental Table 4b). However, the contribution of T to local recycling in the SSE exceeds that of the SMM region by approximately 7% (Supplemental Table 7b). These results suggest that the inconsistencies between T and T-divergence in these two regions are less a function of recycling and more a function of atmospheric circulation. The T-divergence fields indicate that much of the exported T moisture from the SSE region converges in the northeast, while exported SMM T moisture is transported into the Atlantic. Unlike T-divergence, the E-divergence field remains relatively unchanged spatially from the summer to the fall seasons, though the maximum E-divergence shifts from the US west coast to the Great Lakes region (Figure 17k). This shift is consistent with the shift in E from the summer to the fall season (Figure 17j). The largest inconsistency between fall E and E-divergence exists between the NMW and OHV regions. Both regions have low recycling values during the fall (Figures 9a-b) and E contributes a relatively equal percentage of recycling in both regions (Figure 13d). Consistent with the fall T/T-divergence differences, the differences between E and E-divergence are also likely a feature of atmospheric circulation conditions. Fall season C-divergence remains high across southern Canada and the southern/southeastern US, though it drastically decreases from the summer to the fall season in the central/northern US plains (Figure 16k). The main disparities between the C and C-divergence magnitudes occur in the CMM, SMM, NEE, and ALC regions (Figures 16j-k). Each region likely exports moisture out of the North American domain given their proximity to the ocean. Additionally, the fall recycling is considerably higher in CMM and SMM compared to most of the continent (Figures 9a-b) further limiting the C moisture available for export. The contribution of C moisture to local recycling is slightly higher in ALC than the NEE (34% vs 28%) potentially explaining the difference in the C-divergence between these two regions (Figure 13d, Supplemental Table 8b).

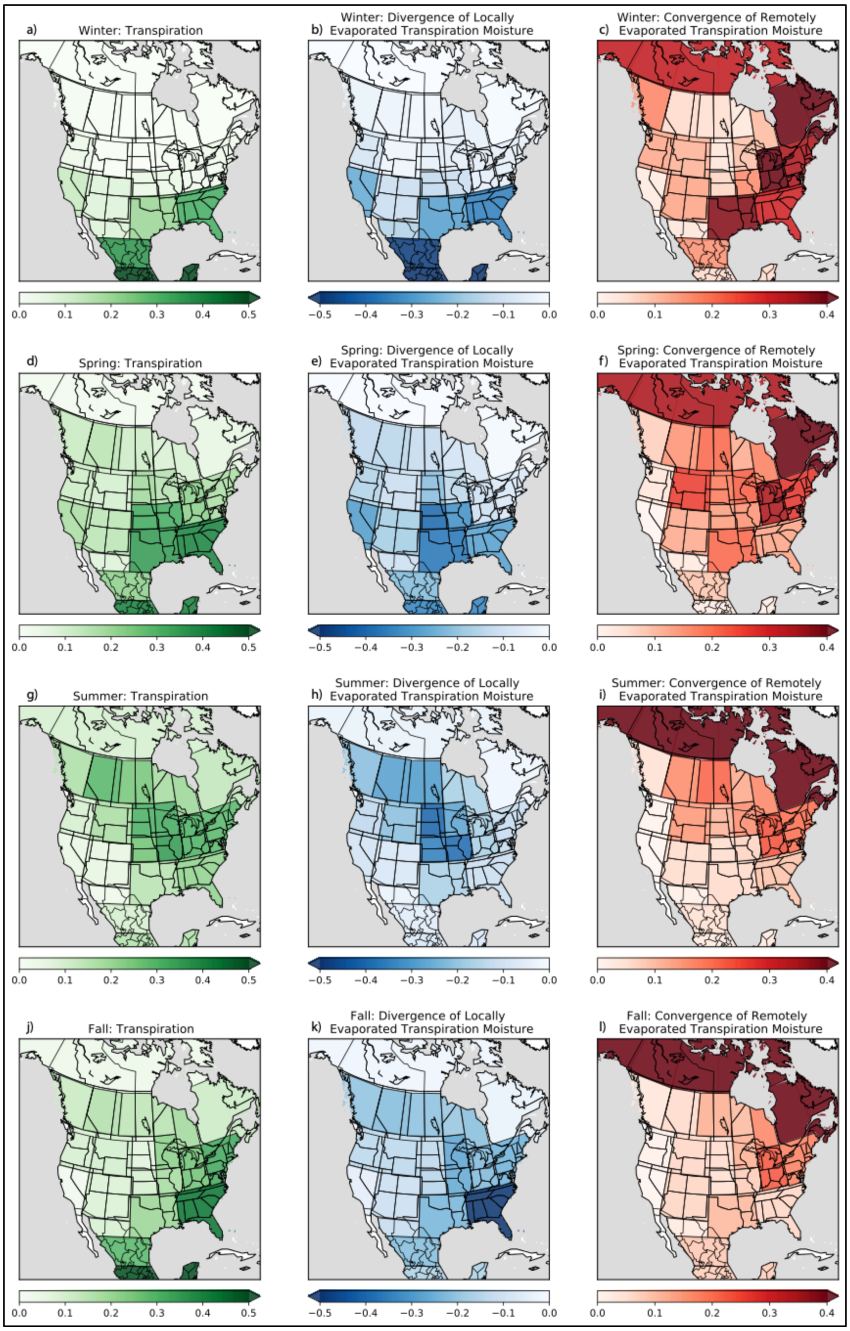

Figure 15. (a) Winter T, (b) winter divergence of locally evaporated T, (c) winter convergence of remotely evaporated T, (d) spring T, (e) spring divergence of locally evaporated T, (f) spring convergence of remotely evaporated T, (g) Summer T, (h) summer divergence of locally evaporated T, (i) summer convergence of remotely evaporated T, (j) Fall T, (k) fall divergence of locally evaporated T, and (l) fall convergence of remotely evaporated T. All units are normalized units of length per m^-1.

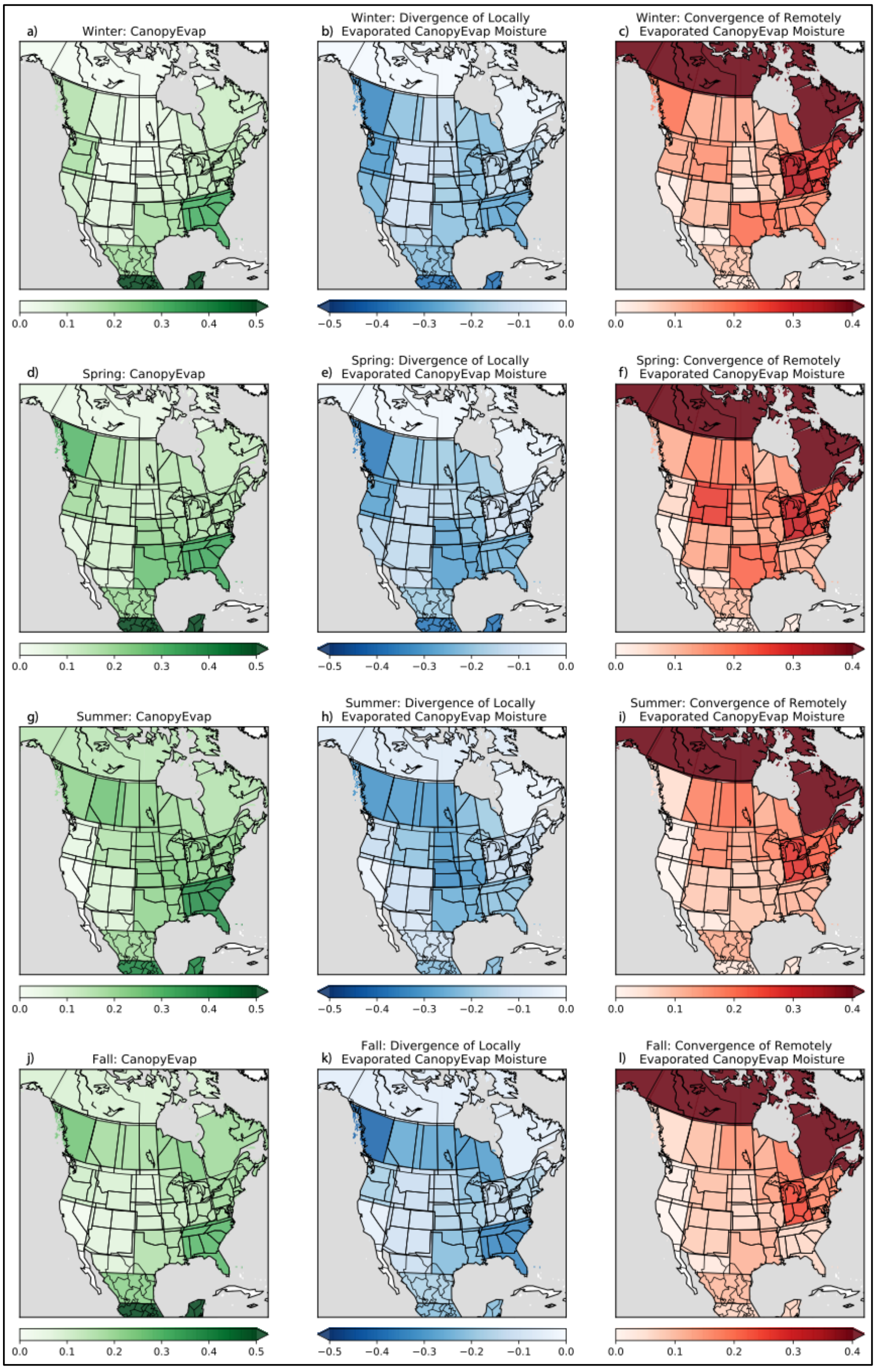

Figure 16. (a) Winter C, (b) winter divergence of locally evaporated C, (c) winter convergence of remotely evaporated C, (d) spring C, (e) spring divergence of locally evaporated C, (f) spring convergence of remotely evaporated C, (g) Summer C, (h) summer divergence of locally evaporated C, (i) summer convergence of remotely evaporated C, (j) Fall C, (k) fall divergence of locally evaporated C, and (l) fall convergence of remotely evaporated C. All units are normalized units of length per m^-1.

https://doi.org/10.5194/hess-2021-284
Preprint. Discussion started: 11 June 2021

Hydrology and Earth System Sciences
Open Access
Discussions

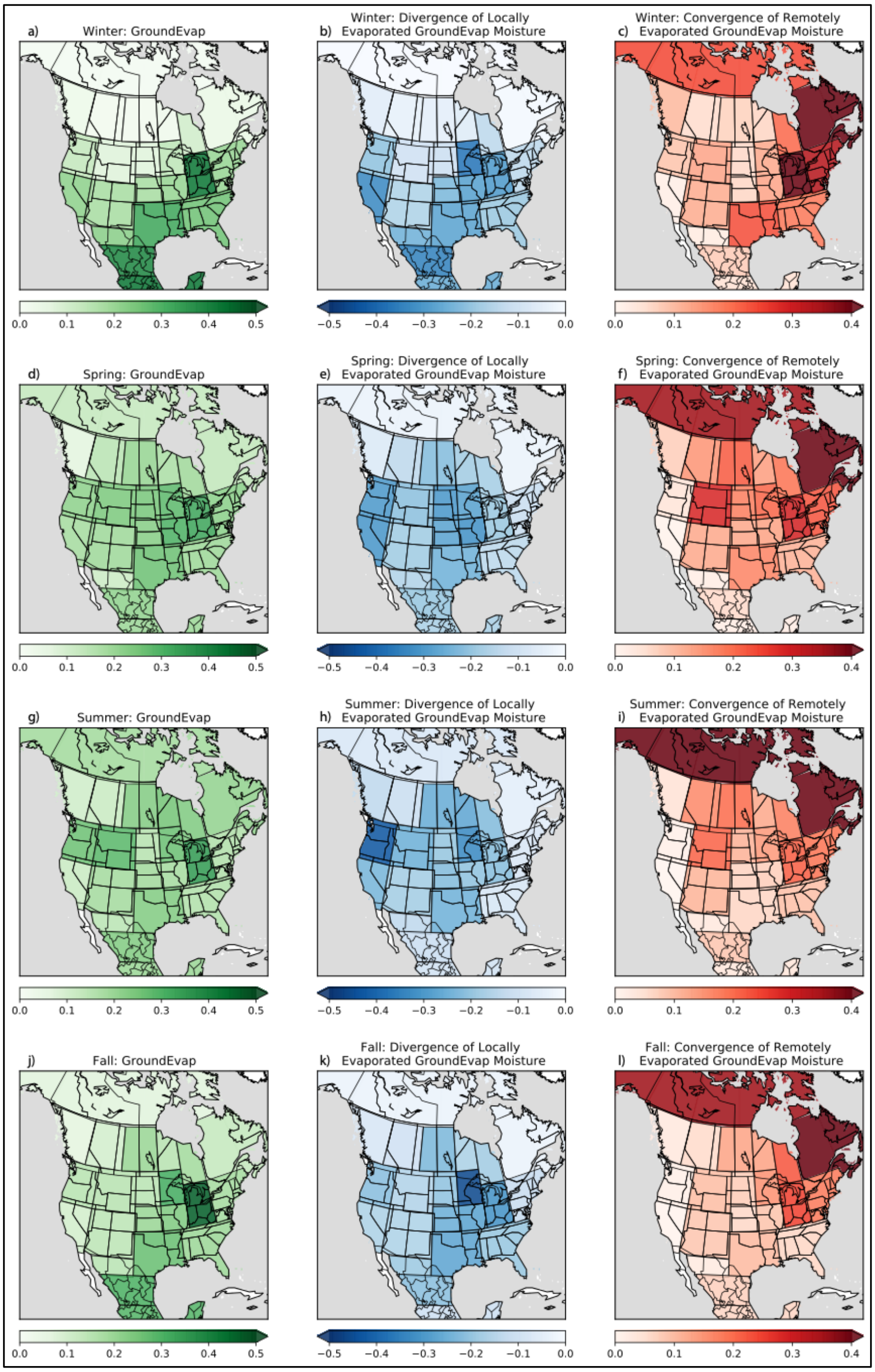

Figure 17. (a) Winter E, (b) winter divergence of locally evaporated E, (c) winter convergence of remotely evaporated E, (d) spring E, (e) spring divergence of locally evaporated E, (f) spring convergence of remotely evaporated E, (g) Summer E, (h) summer divergence of locally evaporated E, (i) summer convergence of remotely evaporated E, (j) Fall E, (k) fall divergence of locally evaporated E, and (l) fall convergence of remotely evaporated E. All units are normalized units of length per m^-1.

https://doi.org/10.5194/hess-2021-284
Preprint. Discussion started: 11 June 2021

4. Discussion:

4.1 The role of T, E, and C in regional precipitation

The online water tracing simulation presented here indicates land surface ET supplies a considerable amount of moisture for precipitation within North America. The extended tracing capabilities in this model simulation, allowing for the explicit tagging of the individual moisture fluxes (T, C, and E), suggests varying contributions both seasonally and spatially from each flux source. The contribution of land surface moisture to total precipitation follows a seasonal cycle with minimum contributions during the winter season (DJF) and maximum contributions during the summer season (JJA) across the entire continent (Figure 4) (Dirmeyer & Brubaker, 2007; Gimeno et al., 2012). In general, land-sourced ET comprises the greatest fraction of total precipitation in the interior portions of North America, where the influence of ocean evaporation is diminished (Figure 4). However, distance from the coastline is clearly not sufficient to explain the heterogeneous spatial patterns of land-sourced precipitation. Instead, these patterns reflect features of the regional atmospheric circulation, topography, and vegetation type and distribution.

During winter, the contribution of terrestrial ET to total precipitation is relatively small across North America due to a lack of photosynthetically active vegetation in the domain, consistent with the relatively high contribution (40 - 60% across much of the continent) of bare ground and lake evaporation (E) to land-sourced precipitation (Figure 4a and Figure 9d). However, land-based precipitation accounts for 15-20% of total precipitation across a southwest-to-northeast oriented swath from Central Mexico to the Great Lakes (Figure 4a). This pattern reflects the substantial land-based moisture transport of ET from Central Mexico and the South Central Plains towards the northeast within the prevailing winter southwesterly flow (as shown in the moisture export analysis), highlighting the key role of these land regions in shaping winter precipitation across a substantial portion of the Central U.S.

As mean temperatures rise in spring, the contribution of terrestrial ET to precipitation increases across North America. In fact, terrestrial ET becomes the dominant source (50-60%) of precipitation in the northern Central Plains of the U.S. and central Canada by this time (Figure 4b). This land-based precipitation maximum is equally sourced from E and T, highlighting the emerging role of vegetation and transpiration by spring (Figure 10b). Indeed, transpiration accounts for 40-50% of precipitation sourced from terrestrial ET for most of North America as early as the spring season.

It is during the summer season however, that terrestrial ET, and in particular, vegetation, becomes the dominant regulating source for much of North America's precipitation (Figure 4c, 14b-c). With the exception of the immediate western coastline, all of North America north of 40°N receives in excess of 50% of their summer precipitation directly from the land surface, with contributions exceeding 70% in much of interior Canada and portions of the northern U.S. Great Plains and Intermountain West (Figure 4c). Similar results were obtained using the Dynamic Recycling Model (DRM) (Dominguez et al., 2006) and using a numerical budget (van der Ent et al., 2010), though we found higher contributions from the land surface further west in CESM. Maximum leaf cross-sectional area and density during summer allows canopy evaporation to become an important source of ET, and therefore precipitation, in much of the U.S. at this time, highlighting the need to monitor and model above ground biomass for accurate prediction of summer precipitation (Figure 11c). For example, if instead of landing on the canopy and evaporating quickly back into the atmosphere, precipitation falls to the soil and infiltrates, the timing and magnitude of ET and subsequent precipitation will be inaccurate. By fall, cooler temperatures and leaf senescence drive a reduced, though still important role for terrestrial ET in shaping precipitation, similar to that in spring (Figure 4d). However, compared to spring, the contribution of transpiration to fall precipitation is smaller across much of North America, while the contribution of canopy evaporation to precipitation is greater (Figure 10 and Figure 12). In other words, the ratio of transpiration to canopy evaporation in fall is smaller than that in spring. This highlights the important role that the existing canopy in the fall season can have on interception and therefore subsequent canopy evaporation and precipitation despite the fact that these plants exhibit reduced photosynthesis and transpiration at this time.

4.2 The role of recycling in shaping regional precipitation

The water tracers utilized in this study tag moisture based on its geographic evaporative origin and on its surface flux pathway (E, T, or C), allowing for a detailed investigation of moisture recycling. In addition to providing information on a region's reliance on remote and proximate moisture for precipitation, the study of each individual ET flux component within the context of recycling reveals key insights into the development of land surface feedbacks that can mitigate or amplify dry and wet periods. The purely physical components of ET (E and C) generally have shorter land surface residence times than the biophysical component of ET (T), and are sourced from reservoirs with minimum water storage capacity (the top soil layer and the surface of vegetation) (van der Ent et al., 2014). In contrast, T has a larger water storage reservoir to draw from and (globally) has a delayed evaporative response to precipitation (van der Ent et al., 2014; Wang-Erlandsson et al., 2014). Therefore, a region that relies on E-based or C-based recycling rather than T-based recycling may be more susceptible to variability in recycling contributions to precipitation. This framework is used to inform the examination and discussion of recycling at the seasonal scale.

During the winter season, appreciable recycling is confined primarily to southern North America within the SCP, CMM, and SMM regions (Figures 5a-b). These three regions largely comprise the southern half of the area of maximum winter land-surface contribution to total precipitation (Figure 4a), further indicating the importance of local-ET for precipitation in this portion of the continent. Given that E moisture dominates moisture recycling in the SCP and CMM regions during winter (Figure 13a), a lack of precipitation could quickly shut off the surface moisture available for local recycling, further reducing precipitation. Since the SMM region receives most locally recycled moisture from T (Figure 13a), recycling may persist during short periods of reduced moisture import/precipitation from other regions, making internal recycling less vulnerable to sudden changes in precipitation, potentially reducing land surface amplification of drying.

During spring, local recycling remains important in Central America and increases in importance across much of the western US, Canadian Prairies, and northern Canada (Figures

5c-d). Though local recycling contributes over 10% of the total precipitation in all of these regions (Supplemental Table 2a), recycling contributes the most to land-based precipitation across the southern US, the US west coast, northern Canada, and Central America (Figures 7a-b). These results indicate that northern Canada, Central America, and the SWW region rely heavily on local ET, while the UPR, WIP, and EIP regions rely heavily on both local and remote terrestrial ET for springtime precipitation. E moisture remains the primary supply of locally recycled moisture in NCA, EIP, UPR, and SWW, while T supplies the most recycled moisture in the CMM, SMM, and WIP regions (Figure 13b). Additionally, E contributes the most to transported moisture in NCA, WIP, EIP, UPR, and SWW, while T supplies the most in CMM and SMM (Figure 14b). This suggests that springtime recycling is highly susceptible to changes in precipitation across much of the western US and Canada, and total precipitation in the UPR and EIP regions is susceptible to both local and remote fluctuations in precipitation. These results are consistent with previous analyses showing that across much of the southern and western portions of North America where moisture availability is the limiting factor for ET, strong correlations exist between soil moisture and ET (Dirmeyer et al., 2008) during the spring season, indicating the need for consistent precipitation to sustain local recycling. Indeed, knowledge of soil moisture in the western US provides predictability of next day precipitation (Tuttle & Salvucci, 2016), further emphasizing the sensitivity of precipitation in the region to local moisture availability. Given that this semi-arid to arid region of North America receives between 20-60% of total springtime precipitation from land surface moisture (Figure 4b), further examining sensitivities to local and remote precipitation changes for these regions will be critical for sustained water resources.

In summer, local recycling is a major supply of land-sourced precipitation across much of the southern and western US, Central America, and northern Canada (Figures 8a-b). Additionally, local recycling supplies over 17% of total precipitation across all of the western US and Canada (except for PFC) (Figures 5e-f, Supplemental Table 3a). In both the UPR and NCA regions, locally sourced ET moisture contributes over 25% of summer rainfall totals (Supplemental Table 3a). Similar summer recycling ratio spatial patterns were found using the DRM in Dominguez et al. (2006), though the DRM produced much higher recycling ratios in the southeastern US compared with the results from our CESM water tracer simulation, likely due to overestimates of ET in the southeast and the reliance on the well-mixed assumption. Since western North America serves as the source of much of its own precipitation in summer, it is highly sensitive to changes in internal recycling. Indeed, summer droughts in the Canadian Prairies are correlated with lower amounts of local recycling (Raddatz, 2005). Regional intensification of drought episodes across the western US have also been strongly linked to a lack of internal moisture recycling (Herrera-Estrada et al., 2019), suggesting that sustained recycling is necessary for drought mitigation. Additionally, many of the agricultural regions of the central US rely on moisture supplies from the southern/western US (Bagley et al., 2012; Herrera-Estrada et al., 2019), indicating the potential for droughts in the west to impact crop yields in one of the world's breadbaskets. In contrast with the spring season, both summer moisture recycling and moisture transport are largely supplied by T sourced moisture in North America (Figure 13c). However, the combination of E and C moisture to local recycling is over 50% in all of these western regions except WIP and EIP (Supplemental Table 7). Since both of these moisture

https://doi.org/10.5194/hess-2021-284
Preprint. Discussion started: 11 June 2021

sources rely on a consistent supply of precipitation, local recycling (and in turn total precipitation) across much of western North America is highly sensitive to changes in local and regional precipitation.

The precipitation contribution from internal local recycling decreases from the summer to the fall season for much of North America. Central America, northern Canada, the EIP, and the SWW regions receive the most precipitation from local ET sources (between 8-9% of total precipitation) (Figures 5g-h, Supplemental Table 4a). Similar to the contribution of local recycling to total precipitation, the contribution of recycling to land-based precipitation also decreases from the summer to the fall across the western US and Canada. The highest contributions of internal recycling to terrestrial sourced precipitation are in the SSE, CMM, and SMM regions (all at or above 40%) (Figures 9a-b, Supplemental Table 4b). Despite reductions in the contributions of local recycling, in the regions where local recycling remains an important source of total rainfall, the land surface still contributes between 20-40% of the moisture for precipitation (Figure 4d). While less impactful than the summer season, fluctuations in local ET supplies during the fall could still have major implications for water supplies in portions of southern North America and western/northern Canada. With the declining vegetation extent during the fall, T contribution to recycling decreases, and E and C moisture dominate (Figure 13d). For regions where local recycling is an important precipitation source (NCA, EIP, SWW, CMM, and SMM), the combination of E and C moisture comprises over 65% of local recycling and 78% in the SWW region alone (Supplemental Table 8). These physical components of ET require a constant source of moisture and evaporative demand by the atmosphere. C in particular requires a constant supply of moisture as rates of C are high during and immediately following precipitation, and asymptotically approach zero just hours after precipitation has ended (Wang-Erlandsson et al., 2014). The lack of T moisture recycling, particularly in the SWW, makes each of these regions vulnerable to changes in local precipitation.

4.3 The role of external moisture in shaping regional precipitation

The mathematical framework developed in Section 2.2 and Appendix A in conjunction with the online water tracers allows for the investigation of important North American sources and sinks of land ET moisture. Specifically, the framework identifies those regions that are critical in supplying moisture to other locations in North America, and those regions that rely heavily on other North American regions for their precipitation. Additionally, by utilizing the individual ET component tracers, we are able to examine the dependence of each region on remote moisture convergence from the different moisture flux sources (E, C, and T), providing insights into potential susceptibility to changes in remote precipitation. We consider regions with a high divergence of locally evaporated moisture (referred to as ET, T, E, or C divergence) as sources of terrestrial moisture and regions with a high convergence of remotely evaporated moisture (referred to as ET, T, E, or C convergence) as sinks of terrestrial moisture. Because our mathematical development of these terms considers only moisture that originates and precipitates within the North America domain, any moisture that evaporates from within North America and is exported out of North America is not considered in the divergence term nor is evaporation from outside North America that precipitates within North America considered in the convergence term. By

https://doi.org/10.5194/hess-2021-284
Preprint. Discussion started: 11 June 2021

Hydrology and Earth System Sciences
Discussions
Open Access

restricting our study domain in this way, we are able to investigate key potential land surface teleconnections within North America and exclude contributions from outside the domain. Deviations between regional ET and the divergence of ET reflect the fact that some ET is exported out of North America, and that some regions exhibit high internal recycling (in both instances divergence values are less than ET values).

ET divergence during the winter season is highest in the southern half of the continent and in the US Great Lakes region (Figure 7b), fairly consistent with the ET evaporation fields (Figure 7a). The corresponding winter convergence fields are highest in magnitude along the east coast, though moderately high values of convergence are present in the western US and the PFC region as well (Figure 7c). The combination of the convergence and divergence fields suggest much of southern North America and portions of the central US supply most of the winter terrestrial-sourced precipitation for the continent.

The convergence fields for the individual ET components are spatially similar to one another, though C and E convergence are slightly higher than T convergence in the western US and Canada, and T convergence is higher than C or E convergence in the southern/ southeastern US (Figures 15-17c). Similarly, T divergence is generally higher in the southern US and Central America, while E convergence is highest near the Great Lakes, and C convergence is highest along the western coast of the US and Canada (Figures 15-17b). These results suggest eastern North America receives high amounts of imported moisture from each ET component. In the far northeast ALC region, where winter moisture import is dominated by E (Figure 14a, Supplemental Table 9), most of that moisture is likely attributable to the divergence of lake evaporation from the Great Lakes region (Figure 20b). Additionally, ice cover in the Great Lakes has declined considerably in recent decades (Wang et al., 2012), and a decline in ice cover is strongly correlated with increased levels of evaporation from the lake surfaces (Mishra et al., 2010), suggesting ALC may see an increase in winter precipitation as global temperatures rise. In contrast with the east coast, imported precipitation (from within North America) in the western US and Canada is dominated by E and C moisture (Figure 14a). Additionally, the divergence in the west is concentrated in the SWC (T and E), the PNW (E and C), and the PFC (C) regions (Figures 15-17b). This suggests the western US and Canada rely on a few key source regions and on moisture fluxes that are highly sensitive to precipitation frequency, making their wintertime terrestrial precipitation vulnerable to changes in upwind winter precipitation.

During the spring season, ET divergence is moderately high across all of North America except for the far northern NCA and ALC regions, indicating increased moisture exchange between different land regions (Figure 7e). Given the convergence and divergence fields, terrestrial ET moisture appears to be generally sourced from regions to the south and west of where the moisture converges, consistent with prevailing winds. This indicates the high spring divergence of ET moisture from Central America is largely connected to the higher convergence in the SCP region, the high divergence along the US west coast is connected to the high convergence in the Canadian Prairies and northwestern US, and the high divergence in the US southern/central plains is connected to the high convergence in the northeast (Figures 7e-f).

https://doi.org/10.5194/hess-2021-284
Preprint. Discussion started: 11 June 2021

The imported precipitation from each ET component source confirms that E is the primary source of imported moisture during spring in western North America (high convergence regions of the UPR, WIP, and EIP), while T is the primary imported moisture source in central and eastern North America (high convergence regions of the SCP, OHV, NEE, and NMW) (Figure 17b, Supplemental Table 10). The eastern ALC and EON regions are exceptions as imported E exceeds that of T (Figure 17b, Supplemental Table 10), though both regions are immediately downwind of the Great Lakes which exhibit high rates of evaporation during the early spring season when the gradient between the air temperature and lake temperature is large (Spence et al., 2013). The important role of canopy evaporation transport also becomes apparent in spring as plants leaf out, contributing to remote precipitation on both sides of the continent (Figure 19f).

The T-, E-, C-convergence results indicate that spring precipitation in the Canadian Prairies and Upper Rockies is likely vulnerable to springtime precipitation changes (those that greatly affect E and C) in remote regions of the US Southwest and along the west coast of the continent. These results are consistent with previous work linking droughts in the UPR and southern EIP/WIP regions to decreased moisture transport from drought-stricken portions of the US West Coast/Southwest (Herrera-Estrada et al., 2019). The T-, E-, C-convergence also reveals the strong connection between transpiration divergence from the south central plains and Southeast U.S. and transpiration convergence in the Northeast U.S., highlighting the far-reaching impact vegetation can have on precipitation. Indeed, previous work has shown that the length scale of T (the distance water molecules travel between the evaporative source region and the location the molecule precipitates) is the largest of the three components (van der Ent et al., 2014). This is likely the case because T-based moisture, compared with E- or C-based moisture, is more likely to enter the atmosphere during periods of dry weather and is therefore less likely to precipitate quickly.

In summer, ET-divergence magnitudes are highest in the central/northern US plains and in the Canadian Prairies indicating that these agricultural hotspots are major suppliers of land moisture for the rest of North America (Figure 7h). The low convergence values across the southern half of North America and along the west coast further indicate local ET is crucial for water supplies given most of these regions still receive between 30-50% of summer precipitation from land surface moisture (Figure 4c).

The summer convergence & divergence fields for the individual ET components reveal several potential land moisture vulnerabilities for the North American continent. The T convergence field is clustered entirely in the north and northeastern portions of the continent (Figure 15i), while the T divergence field magnitudes are drastically higher in the US central/northern plains and in the Canadian Prairies (Figure 15h). These results suggest either land use/management changes (e.g., reduced irrigation) or severe/persistent drought conditions, which stress vegetation and shut down transpiration, in the US and Canadian agricultural regions could drastically reduce precipitation and potentially lead to drought conditions across the north and northeast. Indeed, agricultural droughts have been shown to decrease the moisture transport into the northeast (Herrera-Estrada et al., 2019), and irrigation in the central US has led to enhanced downwind precipitation (DeAngelis et al., 2010). Knowledge of the strong link between transpiration in the central US and

https://doi.org/10.5194/hess-2021-284
Preprint. Discussion started: 11 June 2021

precipitation on the east coast provides a potentially valuable drought monitoring tool. As plants become water stressed they conserve water and transpire less. Indeed, very high correlations exist between the Normalized Difference Vegetation Index (NDVI) (a measure of plant health) and the Standardized Precipitation Index (SPI) (a measure of meteorological drought) across the Northern US Plains during the summer growing season (Ji and Peters, 2003). Plants are most vulnerable to drought conditions during their growing stage when access to water is critical for plant development (Ji & Peters, 2003; Salter & Goode, 1967). Given the extensive history of severe droughts across the central US and Canadian Prairies (Rippey, 2015; Stambaugh et al., 2011; Woodhouse & Overpeck, 1998) and the evidence of increasing drought variability across the region (Zambreski et al., 2018), close monitoring of land surface conditions within the agricultural regions of North America are necessary for drought monitoring in the north/northeast.

The individual ET component tracers also confirm that the south/southwestern portions of North America receive the greatest contributions from E and C moisture to total imported precipitation (Figure 14c, Supplemental Table 11). Not only does this region of North America rely on E and C for moisture import, but as noted previously, local recycling (the primary source of terrestrial precipitation) also relies heavily on C and E (Figure 13c). Without a strong reliance on T, precipitation that falls in prior seasons is less able to buffer against meteorological drought. Therefore, if much of the West experiences a deficit in summer precipitation, drought in the Southwest U.S. could quickly intensify due to a lack of recycling and a lack of regional moisture transport, making this region especially prone to enhanced drought conditions. Paleoclimate records and tree ring analysis has revealed western North America has experienced repeated drought episodes, including megadroughts (multidecadal periods of increased aridity), in the past (Cook et al., 2004). Given the source origins of moisture across the west, events of similar magnitude remain possible in the present climate (Ault et al., 2018).

Unlike the summer season, fall season ET divergence is spread across nearly all of North America, though the highest divergence magnitudes are seen around the Great Lakes and in the south/southeastern US (Figure 7k). ET convergence values are also spread across the continent, but the highest convergence values are clustered in the northeast (Figure 7l). Despite lower land surface moisture contributions during the fall season, ET moisture still supplies 30-50% of the moisture for precipitation (Figure 4d), making land surface teleconnections still critical for water supplies.

The convergence values of each ET component are highest in the northeast as well and lowest in the southern/western portions of the continent (Figures 15-17l). For southern and western North America, E and C convergence values remain higher than T convergence, further indicating these regions rely heavily on E and C moisture. T divergence is strongest in the eastern half of North America and is particularly strong in the SSE region where T is very high during the fall season (Figures 15j-k). Given the strong convergence values to the north of the SSE region, the SSE (along with the immediate surrounding regions) likely supplies the majority of the imported T moisture into the northeast. While the northeast seemingly receives the majority of T convergence from the SSE region alone (a region that experiences several droughts due to both atmospheric and oceanic variability (Schubert et al., 2021; Luo & Wood, 2007; Manuel, 2008)), transpiration often increases in the SSE during droughts to meet the evaporative demand of the atmosphere (Kam et al., 2014). The increased land/atmosphere coupling in the SSE during drought episodes likely helps maintain a constant supply of ET moisture from the SSE, limiting the potential vulnerability of northeastern North America. However, some studies have suggested both an increase in the severity and frequency of droughts in the future in the southeastern US (including our SCP and SSE regions) (Mitra et al., 2018), so the Northeast may become vulnerable in the future if the Southeast remains the primary exporter of Northeast land moisture.

5. Conclusion:

In this study, we utilize the Community Earth System Model with online water tracers to examine the influence of land surface moisture on North American precipitation. Additional water tracing capabilities are implemented in the model to investigate the individual contributions to precipitation from each of the components of ET (T, E, and C). Land surface ET is a vital source of moisture for precipitation in North America throughout the year, particularly during the summer season when the northern and northeastern portions of the continent receive up to 80% of total rainfall from land surface moisture. Though the contributions from the components vary both seasonally and spatially, annual-average contributions show T moisture is the dominant component across the north and east, while E moisture is dominant in the south and west.

The water tracers also allow for the direct investigation of moisture recycling from each defined land region across North America. During the warm seasons (Spring, Summer, Fall), moisture recycling is highest across the western half of the continent with some regions receiving up to 25% of total precipitation from internal recycling. Recycled moisture comes from all three ET components, but like the contributions to precipitation, the contributions of each component to recycling varies by season. E and C are the primary sources of recycled moisture in North America during the winter and fall seasons, while the summer is dominated by T, and the spring receives high contributions from all three components. Across much of western North America where local recycling rates are highest, the recycled moisture is comprised predominantly by E and C, which are both highly sensitive to changes in precipitation frequency. Our results indicate dry conditions in western and southwestern North America could quickly shut off the local recycling, amplifying drought conditions.

Using the water tracers and a matrix formulation of moisture transport, we identify key sources and sinks of land moisture seasonally across North America. In all seasons, eastern and northeastern North America import large quantities of moisture from other North American land regions, though the primary exports of land moisture vary seasonally. We identify potential key land surface teleconnections based on these moisture transport fields. Connections are found between Central America and the southern US, the southern/southeast US and the Northeast, the central plains and the Northeast, the Canadian Prairies and the Northeast, and the west coast and much of the interior western US/Canada. The individual ET component tracers reveal that in general, the connections to the western US/Canada primarily involve exports of C and E moisture, while the connections to the Northeast come

https://doi.org/10.5194/hess-2021-284
Preprint. Discussion started: 11 June 2021

from all three components. Our results indicate that imported precipitation in the interior western US/Canada is vulnerable to concurrent (same season) changes in precipitation along the west coast of the continent. Though the Northeast appears to import moisture from all ET components and from several different regions, land use/management changes (such as changes to irrigation) or severe droughts in the southern US, central plains, or the Canadian Prairies could lead to strong reductions in Northeast precipitation, especially during the warm season.

Our study revealed potential land surface teleconnections and moisture vulnerabilities across North America. While we focused here on the current state of the climate, many uncertainties exist for how these land surface teleconnections will change in the future. There is much uncertainty about the partitioning of ET into its three components under elevated CO_2 levels (Megis et al., 2015; Kirschbaum & McMillan, 2018). A longer growing season and increased leaf-area index (LAI) could enhance T (Niu et al., 2019), while increased CO_2 levels could decrease plant stomatal conductance, increase plant water-use efficiency, and decrease T (Lammertsma et al., 2011). Changes in the partitioning of ET could significantly alter the precipitation teleconnections presented in this study and the resulting vulnerabilities we identified. Additionally, many of the vulnerabilities we identified point to droughts in upwind land moisture sources as a mechanism for reducing moisture transport. Studies have suggested an increase in potential evapotranspiration in future climates leading to more intense and longer-duration droughts across most of the US and southern Canada (Jeong et al., 2014). Atmospheric moisture demand is also expected to increase in the future, potentially leading to persistent droughts across the US (Dai, 2010). Increased aridity and persistent drought episodes could enhance the vulnerabilities we have identified (assuming these land surface teleconnections remain in the future climate). Future studies are needed to identify how land surface teleconnections will change in future climates and how increased aridity will affect those teleconnections.

https://doi.org/10.5194/hess-2021-284
Preprint. Discussion started: 11 June 2021

Appendix A: Domain Restriction Scaling for E = P

Here we show the scaling factor needed to restrict the domain of Equation (2) in Section 2.2. We know that on a global domain, $\overline{\mathrm{E}} = \overline{\mathrm{P}}$. Let us divide the global domain D with three disjoint partitions such that $D = D_1 + D_2 + D_3$.

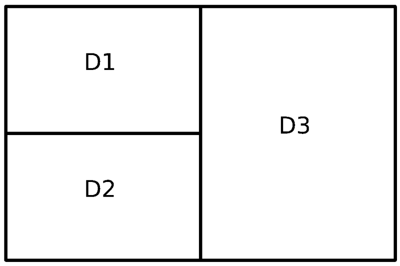

Using this domain,

$$\overline{P_D} = \overline{E_D} \qquad (1)$$

Since the partitions of D are disjoint, we can express the total $\overline{\mathrm{E}}_{\mathrm{D}}$ and $\overline{\mathrm{P}}_{\mathrm{D}}$ variables as a weighted average of the partitions such that

$$\overline{E_D} = \overline{E_{D1}}(\frac{\alpha_{D1}}{\alpha_D}) + \overline{E_{D2}}(\frac{\alpha_{D2}}{\alpha_D}) + \overline{E_{D3}}(\frac{\alpha_{D3}}{\alpha_D}) = \overline{P_{D1}}(\frac{\alpha_{D1}}{\alpha_D}) + \overline{P_{D2}}(\frac{\alpha_{D2}}{\alpha_D}) + \overline{P_{D3}}(\frac{\alpha_{D3}}{\alpha_D}) = \overline{P_D} \qquad (2)$$

where α represents the area of the domain.

We know that all of the available E that can be converted into P must be contained within the closed set {D}. The $\overline{\mathrm{P}}$ for each partition can be written as a linear combination of evaporated moisture from each partition of D:

$$\overline{P_{D1}}(\frac{\alpha_{D1}}{\alpha_D}) = \overline{E_{D1}}(\frac{\alpha_{D1}}{\alpha_D})(\lambda_{11}) + \overline{E_{D2}}(\frac{\alpha_{D2}}{\alpha_D})(\lambda_{21}) + \overline{E_{D3}}(\frac{\alpha_{D3}}{\alpha_D})(\lambda_{31}) \qquad (3)$$

$$\overline{P_{D2}}(\frac{\alpha_{D2}}{\alpha_D}) = \overline{E_{D1}}(\frac{\alpha_{D1}}{\alpha_D})(\lambda_{12}) + \overline{E_{D2}}(\frac{\alpha_{D2}}{\alpha_D})(\lambda_{22}) + \overline{E_{D3}}(\frac{\alpha_{D3}}{\alpha_D})(\lambda_{32}) \qquad (4)$$

$$\overline{P_{D3}}(\frac{\alpha_{D3}}{\alpha_D}) = \overline{E_{D1}}(\frac{\alpha_{D1}}{\alpha_D})(\lambda_{13}) + \overline{E_{D2}}(\frac{\alpha_{D2}}{\alpha_D})(\lambda_{23}) + \overline{E_{D3}}(\frac{\alpha_{D3}}{\alpha_D})(\lambda_{33}) \qquad (5)$$

https://doi.org/10.5194/hess-2021-284
Preprint. Discussion started: 11 June 2021

where λ_{ij} is the fraction of precipitation from partition i that falls in partition j. Note that for any region i, the sum of all λ's must equal one

$$\sum_{j=1}^{n} \lambda_{ij} = 1 \qquad (6)$$

Placing equations (3)-(5) into equation (2), we obtain the following equality:

$$\overline{E_D} = \overline{E_{D1}}(\frac{\alpha_{D1}}{\alpha_D}) + \overline{E_{D2}}(\frac{\alpha_{D2}}{\alpha_D}) + \overline{E_{D3}}(\frac{\alpha_{D3}}{\alpha_D}) =$$

$$\begin{aligned}
&\overline{E_{D1}}(\frac{\alpha_{D1}}{\alpha_D})(\lambda_{11}) + \overline{E_{D2}}(\frac{\alpha_{D2}}{\alpha_D})(\lambda_{21}) + \overline{E_{D3}}(\frac{\alpha_{D3}}{\alpha_D})(\lambda_{31}) + \\
&\overline{E_{D1}}(\frac{\alpha_{D1}}{\alpha_D})(\lambda_{12}) + \overline{E_{D2}}(\frac{\alpha_{D2}}{\alpha_D})(\lambda_{22}) + \overline{E_{D3}}(\frac{\alpha_{D3}}{\alpha_D})(\lambda_{32}) + \\
&\overline{E_{D1}}(\frac{\alpha_{D1}}{\alpha_D})(\lambda_{13}) + \overline{E_{D2}}(\frac{\alpha_{D2}}{\alpha_D})(\lambda_{23}) + \overline{E_{D3}}(\frac{\alpha_{D3}}{\alpha_D})(\lambda_{33}) =
\end{aligned}$$

$$\overline{P_{D1}}(\frac{\alpha_{D1}}{\alpha_D}) + \overline{P_{D2}}(\frac{\alpha_{D2}}{\alpha_D}) + \overline{P_{D3}}(\frac{\alpha_{D3}}{\alpha_D}) = \overline{P_D} \qquad (7)$$

If we restrict our domain of interest to include D_1 and D_2 only, several terms can be removed from equation (7). If our domain does not include D_3, both the evaporation from and the precipitation within D_3 must be subtracted out of equation (7). To remove all of the evaporation, each term with E_{D3} is subtracted out, and to remove all of the precipitation, each term with λ_{i3} is subtracted out. Recall that

$$\overline{E_{D3}}(\frac{\alpha_{D3}}{\alpha_D}) = \overline{E_{D3}}(\frac{\alpha_{D3}}{\alpha_D})(\lambda_{31}) + \overline{E_{D3}}(\frac{\alpha_{D3}}{\alpha_D})(\lambda_{32}) + \overline{E_{D3}}(\frac{\alpha_{D3}}{\alpha_D})(\lambda_{33}) \qquad (8)$$

$$\overline{P_{D3}}(\frac{\alpha_{D3}}{\alpha_D}) = \overline{E_{D1}}(\frac{\alpha_{D3}}{\alpha_D})(\lambda_{13}) + \overline{E_{D2}}(\frac{\alpha_{D3}}{\alpha_D})(\lambda_{23}) + \overline{E_{D3}}(\frac{\alpha_{D3}}{\alpha_D})(\lambda_{33}) \qquad (9)$$

After subtracting the five terms from each side of the equality in equation (7), we are left with the following

https://doi.org/10.5194/hess-2021-284
Preprint. Discussion started: 11 June 2021

$$\begin{aligned}
\overline{E_D} - \overline{E_{D3}}(\frac{\alpha_{D3}}{\alpha_D}) - \overline{E_{D1}}(\frac{\alpha_{D1}}{\alpha_D})(\lambda_{13}) - \overline{E_{D2}}(\frac{\alpha_{D2}}{\alpha_D})(\lambda_{23}) = \\
\overline{E_{D1}}(\frac{\alpha_{D1}}{\alpha_D}) + \overline{E_{D2}}(\frac{\alpha_{D2}}{\alpha_D}) - \overline{E_{D1}}(\frac{\alpha_{D1}}{\alpha_D})(\lambda_{13}) - \overline{E_{D2}}(\frac{\alpha_{D2}}{\alpha_D})(\lambda_{23}) = \\
\overline{E_{D1}}(\frac{\alpha_{D1}}{\alpha_D})(\lambda_{11}) + \overline{E_{D1}}(\frac{\alpha_{D1}}{\alpha_D})(\lambda_{12}) + \overline{E_{D2}}(\frac{\alpha_{D2}}{\alpha_D})(\lambda_{21}) + \overline{E_{D2}}(\frac{\alpha_{D2}}{\alpha_D})(\lambda_{22}) = \\
\overline{P_{D1}}(\frac{\alpha_{D1}}{\alpha_D}) + \overline{P_{D2}}(\frac{\alpha_{D2}}{\alpha_D}) - \overline{E_{D3}}(\frac{\alpha_{D3}}{\alpha_D})(\lambda_{31}) - \overline{E_{D3}}(\frac{\alpha_{D3}}{\alpha_D})(\lambda_{32}) = \\
\overline{P_D} - \overline{P_{D3}}(\frac{\alpha_{D3}}{\alpha_D}) - \overline{E_{D3}}(\frac{\alpha_{D3}}{\alpha_D})(\lambda_{31}) - \overline{E_{D3}}(\frac{\alpha_{D3}}{\alpha_D})(\lambda_{32}) \qquad (10)
\end{aligned}$$

Isolating and re-writing the third and fourth lines of equation (10) leaves us with

$$\begin{aligned}
\overline{P_{D1}}(\frac{\alpha_{D1}}{\alpha_D})(\lambda_{11} + \lambda_{12}) + \overline{P_{D2}}(\frac{\alpha_{D2}}{\alpha_D})(\lambda_{21} + \lambda_{22}) = \\
\overline{E_{D1}}(\frac{\alpha_{D1}}{\alpha_D})(\lambda_{11} + \lambda_{12}) + \overline{E_{D2}}(\frac{\alpha_{D2}}{\alpha_D})(\lambda_{21} + \lambda_{22}) \qquad (11)
\end{aligned}$$

This straightforward result confirms the equality of E and P (using the assumptions introduced in Section 2) on limited subdomains. This result can also be easily expanded to include n partitions of D such that

$$\sum_{m=1}^{n}\left(\overline{P_{Dm}}(\frac{\alpha_{Dm}}{\alpha_D})(\lambda_{1m} + \lambda_{2m} + ... + \lambda_{nm})\right) = \sum_{m=1}^{n}\left(\overline{E_{Dm}}(\frac{\alpha_{Dm}}{\alpha_D})(\lambda_{1m} + \lambda_{2m} + ... + \lambda_{nm})\right) \qquad (12)$$

resulting in

$$\vec{\ddot{E}} = \begin{bmatrix} \overline{E}_{D1}(\frac{\alpha_{D1}}{\alpha_D})(\lambda_{11} + \lambda_{21} + ... + \lambda_{n1}) \\ \overline{E}_{D2}(\frac{\alpha_{D2}}{\alpha_D})(\lambda_{12} + \lambda_{22} + ... + \lambda_{n2}) \\ . \\ . \\ . \\ \overline{E}_{Dn}(\frac{\alpha_{Dn}}{\alpha_D})(\lambda_{1n} + \lambda_{2n} + ... + \lambda_{nn}) \end{bmatrix} \qquad \vec{\ddot{P}} = \begin{bmatrix} \overline{P}_{D1}(\frac{\alpha_{D1}}{\alpha_D})(\lambda_{11} + \lambda_{21} + ... + \lambda_{n1}) \\ \overline{P}_{D2}(\frac{\alpha_{D2}}{\alpha_D})(\lambda_{12} + \lambda_{22} + ... + \lambda_{n2}) \\ . \\ . \\ . \\ \overline{P}_{Dn}(\frac{\alpha_{Dn}}{\alpha_D})(\lambda_{1n} + \lambda_{2n} + ... + \lambda_{nn}) \end{bmatrix} \qquad (13)$$

https://doi.org/10.5194/hess-2021-284
Preprint. Discussion started: 11 June 2021

When implementing equation (12-13) through the use of water tracers, the precipitation component is simply the weighted average precipitation in the domain of interest from the domain of interest (D1 and D2). The evaporation component requires the additional scaling term to account for evaporation from within the region of interest (D1 or D2) that precipitates outside the domain of interest (D3).

Code and Data Availability

All code and model output used in this manuscript are available from the corresponding author upon a reasonable request.

Author Contributions

T.S.H. and C.B.S. designed the study; T.S.H. performed the analysis; T.S.H. and C.B.S. wrote the manuscript. All authors were involved in setting up the simulation and in editing the manuscript.

Competing Interests

The authors declare no competing interests.

Acknowledgments

The CESM project is supported primarily by the National Science Foundation (NSF). This material is based upon work supported by the National Center for Atmospheric Research, which is a major facility sponsored by the NSF under Cooperative Agreement No. 1852977. Computing and data storage resources, including the Cheyenne supercomputer (doi:10.5065/D6RX99HX), were provided by the Computational and Information Systems Laboratory (CISL) at NCAR. We thank all the scientists, software engineers, and administrators who contributed to the development of CESM1.

Literature Cited

Adler, R. F., Gu, G., Huffman, G. J., Sapiano, M. R., & Wang, J.-J. (2020). GPCP and the Global Characteristics of Precipitation. *Advances in Global Change Research*, 677–697. doi:10.1007/978-3-030-35798-6_11

Alter, R. E., Douglas, H. C., Winter, J. M., & Eltahir, E. A. (2018). Twentieth Century Regional Climate Change During the Summer in the Central United States Attributed to Agricultural Intensification. *Geophysical Research Letters*, *45*(3), 1586–1594. doi:10.1002/2017gl075604

Ault, T. R., St. George, S., Smerdon, J. E., Coats, S., Mankin, J. S., Carrillo, C. M., et al. (2018). A Robust Null Hypothesis for the Potential Causes of Megadrought in Western North America. *Journal of Climate*, *31*(1), 3–24. doi:10.1175/jcli-d-17-0154.1

Bagley, J. E., Desai, A. R., Dirmeyer, P. A., & Foley, J. A. (2012). Effects of land cover change on moisture availability and potential crop yield in the world's breadbaskets. *Environmental Research Letters*, *7*(1), 014009. doi:10.1088/1748-9326/7/1/014009

Brady, E., Stevenson, S., Bailey, D., Liu, Z., Noone, D., Nusbaumer, J., et al. (2019). The Connected Isotopic Water Cycle in the Community Earth System Model Version 1. *Journal of Advances in Modeling Earth Systems*, *11*(8), 2547–2566. doi:10.1029/2019ms001663

Cook, E. R., Woodhouse, C. A., Eakin, C. M., Meko, D. M., & Stahle, D. W. (2004). Long-Term Aridity Changes in the Western United States. *Science*, *306*(5698), 1015–1018. doi:10.1126/science.1102586

Dai, A. (2011). Drought under global warming: a review. *Wiley Interdisciplinary Reviews: Climate Change*, *2*(1), 45–65. doi:10.1002/wcc.81

DeAngelis, A., Dominguez, F., Fan, Y., Robock, A., Kustu, M. D., & Robinson, D. (2010). Evidence of enhanced precipitation due to irrigation over the Great Plains of the United States. *Journal of Geophysical Research*, *115*(D15). doi:10.1029/2010jd013892

Dirmeyer, P. A., & Brubaker, K. L. (1999). Contrasting evaporative moisture sources during the drought of 1988 and the flood of 1993. *Journal of Geophysical Research: Atmospheres*, *104*(D16), 19383–19397. doi:10.1029/1999jd900222

Dirmeyer, P. A., & Brubaker, K. L. (2007). Characterization of the Global Hydrologic Cycle from a Back-Trajectory Analysis of Atmospheric Water Vapor. *Journal of Hydrometeorology*, *8*(1), 20–37. doi:10.1175/jhm557.1

Dirmeyer, P. A., Schlosser, C. A., & Brubaker, K. L. (2009). Precipitation, Recycling, and Land Memory: An Integrated Analysis. *Journal of Hydrometeorology*, *10*(1), 278–288. doi:10.1175/2008jhm1016.1

Dominguez, F., Kumar, P., Liang, X.-Z., & Ting, M. (2006). Impact of Atmospheric Moisture Storage on Precipitation Recycling. *Journal of Climate*, *19*(8), 1513–1530. doi:10.1175/jcli3691.1

Findell, K. L., Keys, P. W., van der Ent, R. J., Lintner, B. R., Berg, A., & Krasting, J. P. (2019). Rising Temperatures Increase Importance of Oceanic Evaporation as a Source for Continental Precipitation. *Journal of Climate*, *32*(22), 7713–7726. doi:10.1175/jcli-d-19-0145.1

Gimeno, L., Stohl, A., Trigo, R. M., Dominguez, F., Yoshimura, K., Yu, L., et al. (2012). Oceanic and terrestrial sources of continental precipitation. *Reviews of Geophysics*, *50*(4). doi:10.1029/2012rg000389

Good, S. P., Noone, D., & Bowen, G. (2015). Hydrologic connectivity constrains partitioning of global terrestrial water fluxes. *Science*, *349*(6244), 175–177. doi:10.1126/science.aaa5931

Herrera-Estrada, J. E., Martinez, J. A., Dominguez, F., Findell, K. L., Wood, E. F., & Sheffield, J. (2019). Reduced Moisture Transport Linked to Drought Propagation Across North America. *Geophysical Research Letters*, *46*(10), 5243–5253. doi:10.1029/2019gl082475

Hua, L., Zhong, L., & Ke, Z. (2016). Precipitation recycling and soil-precipitation interaction across the arid and semi-arid regions of China. *International Journal of Climatology*, *36*(11), 3708–3722. doi:10.1002/joc.4586

Hurrell, J. W., Holland, M. M., Gent, P. R., Ghan, S., Kay, J. E., Kushner, P. J., et al. (2013). The Community Earth System Model: A Framework for Collaborative Research. *Bulletin of the American Meteorological Society*, *94*(9), 1339–1360. doi:10.1175/bams-d-12-00121.1

Jeong, D. I., Sushama, L., & Naveed Khaliq, M. (2014). The role of temperature in drought projections over North America. *Climatic Change*, *127*(2), 289–303. doi:10.1007/s10584-014-1248-3

Ji, L., & Peters, A. J. (2003). Assessing vegetation response to drought in the northern Great Plains using vegetation and drought indices. *Remote Sensing of Environment*, *87*(1), 85–98. doi:10.1016/s0034-4257(03)00174-3

Kam, J., Sheffield, J., & Wood, E. F. (2014). A multiscale analysis of drought and pluvial mechanisms for the Southeastern United States. *Journal of Geophysical Research: Atmospheres*, *119*(12), 7348–7367. doi:10.1002/2014jd021453

Kelemen, F. D., Ludwig, P., Reyers, M., Ulbrich, S., & Pinto, J. G. (2016). Evaluation of moisture sources for the Central European summer flood of May/June 2013 based on regional climate model simulations. *Tellus A: Dynamic Meteorology and Oceanography*, *68*(1), 29288. doi:10.3402/tellusa.v68.29288

Keys, P. W., Wang-Erlandsson, L., & Gordon, L. J. (2016). Revealing Invisible Water: Moisture Recycling as an Ecosystem Service. *PLOS ONE*, *11*(3). doi:10.1371/journal.pone.0151993

Kirschbaum, M. U. (2004). Direct and Indirect Climate Change Effects on Photosynthesis and Transpiration. *Plant Biology*, *6*(3), 242–253. doi:10.1055/s-2004-820883

Kirschbaum, M. U., & McMillan, A. M. (2018). Warming and Elevated CO2 Have Opposing Influences on Transpiration. Which is more Important? *Current Forestry Reports*, *4*(2), 51–71. doi:10.1007/s40725-018-0073-8

Kopparla, P., Fischer, E. M., Hannay, C., & Knutti, R. (2013). Improved simulation of extreme precipitation in a high-resolution atmosphere model. *Geophysical Research Letters*, *40*(21), 5803–5808. doi:10.1002/2013gl057866

Lammertsma, E. I., Boer, H. J., Dekker, S. C., Dilcher, D. L., Lotter, A. F., & Wagner-Cremer, F. (2011). Global CO2 rise leads to reduced maximum stomatal conductance in Florida vegetation. *Proceedings of the National Academy of Sciences*, *108*(10), 4035–4040. doi:10.1073/pnas.1100371108

Lawrence, D. M., Thornton, P. E., Oleson, K. W., & Bonan, G. B. (2007). The Partitioning of Evapotranspiration into Transpiration, Soil Evaporation, and Canopy Evaporation in a GCM: Impacts on Land–Atmosphere Interaction. *Journal of Hydrometeorology*, *8*(4), 862–880. doi:10.1175/jhm596.1

Li, L., Wang, Y., Arora, V. K., Eamus, D., Shi, H., Li, J., et al. (2018). Evaluating Global Land Surface Models in CMIP5: Analysis of Ecosystem Water- and Light-Use Efficiencies and Rainfall Partitioning. *Journal of Climate*, *31*(8), 2995–3008. doi:10.1175/jcli-d-16-0177.1

Lian, X., Piao, S., Huntingford, C., Li, Y., Zeng, Z., Wang, X., et al. (2018). Partitioning global land evapotranspiration using CMIP5 models constrained by observations. *Nature Climate Change*, *8*(7), 640–646. doi:10.1038/s41558-018-0207-9

Lo, M. H., & Famiglietti, J. S. (2013). Irrigation in California's Central Valley strengthens the southwestern U.S. water cycle. *Geophysical Research Letters*, *40*(2), 301–306. doi:10.1002/grl.50108

Luo, L., & Wood, E. F. (2007). Monitoring and predicting the 2007 US drought. *Geophysical Research Letters*, *34*(22), L22702. doi:doi:10.1029/2007GL031673.

Manuel, J. (2008). Drought in the Southeast: Lessons for Water Management. *Environmental Health Perspectives*, *116*(4). doi:10.1289/ehp.116-a168

Martens, B., Miralles, D. G., Lievens, H., van der Schalie, R., de Jeu, R. A., Fernández-Prieto, D., et al. (2017). GLEAM v3: satellite-based land evaporation and root-zone soil moisture. *Geoscientific Model Development*, *10*(5), 1903–1925. doi:10.5194/gmd-10-1903-2017

Mehran, A., & AghaKouchak, A. (2013). Capabilities of satellite precipitation datasets to estimate heavy precipitation rates at different temporal accumulations. *Hydrological Processes*, *28*(4), 2262–2270. doi:10.1002/hyp.9779

Mehran, A., AghaKouchak, A., & Phillips, T. J. (2014). Evaluation of CMIP5 continental precipitation simulations relative to satellite-based gauge-adjusted observations. *Journal of Geophysical Research: Atmospheres*, *119*(4), 1695–1707. doi:10.1002/2013jd021152

Mercado, L. M., Bellouin, N., Sitch, S., Boucher, O., Huntingford, C., Wild, M., & Cox, P. M. (2009). Impact of changes in diffuse radiation on the global land carbon sink. *Nature*, *458*(7241), 1014–1017. doi:10.1038/nature07949

Miralles, D. G., Gentine, P., Seneviratne, S. I., & Teuling, A. J. (2018). Land-atmospheric feedbacks during droughts and heatwaves: state of the science and current challenges. *Annals of the New York Academy of Sciences*, *1436*(1), 19–35. doi:10.1111/nyas.13912

Miralles, D. G., Jiménez, C., Jung, M., Michel, D., Ershadi, A., McCabe, M. F., et al. (2016). The WACMOS-ET project – Part 2: Evaluation of global terrestrial evaporation data sets. *Hydrology and Earth System Sciences*, *20*(2), 823–842. doi:10.5194/hess-20-823-2016

Mishra, V., Cherkauer, K. A., Bowling, L. C., & Huber, M. (2011). Lake Ice phenology of small lakes: Impacts of climate variability in the Great Lakes region. *Global and Planetary Change*, *76*(3-4), 166–185. doi:10.1016/j.gloplacha.2011.01.004

Mitra, S., Srivastava, P., & Lamba, J. (2018). Probabilistic assessment of projected climatological drought characteristics over the Southeast USA. *Climatic Change*, *147*(3-4), 601–615. doi:10.1007/s10584-018-2161-y

Mueller, B., & Seneviratne, S. I. (2014). Systematic land climate and evapotranspiration biases in CMIP5 simulations. *Geophysical Research Letters*, *41*(1), 128–134. doi:10.1002/2013gl058055

Niu, Z., He, H., Zhu, G., Ren, X., Zhang, L., Zhang, K., et al. (2019). An increasing trend in the ratio of transpiration to total terrestrial evapotranspiration in China from 1982 to 2015 caused by greening and warming. *Agricultural and Forest Meteorology*, *279*, 107701. doi:10.1016/j.agrformet.2019.107701

Nusbaumer, J., & Noone, D. (2018). Numerical Evaluation of the Modern and Future Origins of Atmospheric River Moisture Over the West Coast of the United States. *Journal of Geophysical Research: Atmospheres*, *123*(12), 6423–6442. doi:10.1029/2017jd028081

Paul, S., Ghosh, S., Oglesby, R., Pathak, A., Chandrasekharan, A., & Ramsankaran, R. A. A. J. (2016). Weakening of Indian Summer Monsoon Rainfall due to Changes in Land Use Land Cover. *Scientific Reports*, *6*(1). doi:10.1038/srep32177

Peixoto, J. P., & Oort, A. H. (1992). *Physics of climate*. New York: American Institute of Physics AIP.

Qiu, J., Crow, W. T., Dong, J., & Nearing, G. S. (2020). Model representation of the coupling between evapotranspiration and soil water content at different depths. *Hydrology and Earth System Sciences*, *24*(2), 581–594. doi:10.5194/hess-24-581-2020

Raddatz, R. L. (2005). Moisture recycling on the Canadian Prairies for summer droughts and pluvials from 1997 to 2003. *Agricultural and Forest Meteorology*, *131*(1-2), 13–26. doi:10.1016/j.agrformet.2005.04.007

Rayner, N. A. (2003). Global analyses of sea surface temperature, sea ice, and night marine air temperature since the late nineteenth century. *Journal of Geophysical Research*, *108*(D14). doi:10.1029/2002jd002670

Rippey, B. R. (2015). The U.S. drought of 2012. *Weather and Climate Extremes*, *10A*, 57–64. doi:https://doi.org/10.1016/j.wace.2015.10.004

Roy, T., Martinez, J. A., Herrera-Estrada, J. E., Zhang, Y., Dominguez, F., Berg, A., et al. (2019). Role of Moisture Transport and Recycling in Characterizing Droughts: Perspectives from Two Recent U.S. Droughts and the CFSv2 System. *Journal of Hydrometeorology*, *20*(1), 139–154. doi:10.1175/jhm-d-18-0159.1

Salter, P. J., & Goode, J. E. (1967). Crop Responses to Water at Different Stages of Growth. *The Quarterly Review of Biology*, *44*(4), 421–422.

Schubert, S. D., Chang, Y., DeAngelis, A. M., Wang, H., & Koster, R. D. (2021). On the Development and Demise of the Fall 2019 Southeast U.S. Flash Drought: Links to an Extreme Positive IOD. *Journal of Climate*, *34*(5), 1701–1723. doi:10.1175/jcli-d-20-0428.1

Schubert, S. D., Chang, Y., DeAngelis, A. M., Wang, H., & Koster, R. D. (2021). On the development and demise of the fall 2019 southeast u.s. flash drought: Links to an extreme positive iod. *Journal of Climate*, *34*(5), 1701–1723. doi:10.1175/jcli-d-20-0428.1

Seneviratne, S. I., Corti, T., Davin, E. L., Hirschi, M., Jaeger, E. B., Lehner, I., et al. (2010). Investigating soil moisture–climate interactions in a changing climate: A review. *Earth-Science Reviews*, *99*(3-4), 125–161. doi:10.1016/j.earscirev.2010.02.004

Sheffield, J., Barrett, A. P., Colle, B., Nelun Fernando, D., Fu, R., Geil, K. L., et al. (2013). North American Climate in CMIP5 Experiments. Part I: Evaluation of Historical Simulations of Continental and Regional Climatology. *Journal of Climate*, *26*(23), 9209–9245. doi:10.1175/jcli-d-12-00592.1

Singh, H. A., Bitz, C. M., Nusbaumer, J., & Noone, D. C. (2016). A mathematical framework for analysis of water tracers: Part 1: Development of theory and application to the preindustrial mean state. *Journal of Advances in Modeling Earth Systems*, *8*(2), 991–1013. doi:10.1002/2016ms000649

Sodemann, H., Schwierz, C., & Wernli, H. (2008). Interannual variability of Greenland winter precipitation sources: Lagrangian moisture diagnostic and North Atlantic Oscillation influence. *Journal of Geophysical Research*, *113*(D3). doi:10.1029/2007jd008503

Sorooshian, S., AghaKouchak, A., Arkin, P., Eylander, J., Foufoula-Georgiou, E., Harmon, R., et al. (2011). Advanced Concepts on Remote Sensing of Precipitation at Multiple Scales.

https://doi.org/10.5194/hess-2021-284
Preprint. Discussion started: 11 June 2021

Bulletin of the American Meteorological Society, *92*(10), 1353–1357. doi:10.1175/2011bams3158.1

Stambaugh, M. C., Guyette, R. P., McMurry, E. R., Cook, E. R., Meko, D. M., & Lupo, A. R. (2011). Drought duration and frequency in the U.S. Corn Belt during the last millennium (AD 992–2004). *Agricultural and Forest Meteorology*, *151*(2), 154–162. doi:10.1016/j.agrformet.2010.09.010

Tapiador, F. J., Navarro, A., Levizzani, V., García-Ortega, E., Huffman, G. J., Kidd, C., et al. (2017). Global precipitation measurements for validating climate models. *Atmospheric Research*, *197*, 1–20. doi:10.1016/j.atmosres.2017.06.021

Thomson, A. M., Calvin, K. V., Smith, S. J., Kyle, G. P., Volke, A., Patel, P., et al. (2011). RCP4.5: a pathway for stabilization of radiative forcing by 2100. *Climatic Change*, *109*(1-2), 77–94. doi:10.1007/s10584-011-0151-4

Trenberth, K. E. (1999). Atmospheric Moisture Recycling: Role of Advection and Local Evaporation. *Journal of Climate*, *12*(5), 1368–1381. doi:10.1175/1520-0442(1999)012<1368:amrroa>2.0.co;2

Tuttle, S., & Salvucci, G. (2016). Empirical evidence of contrasting soil moisture-precipitation feedbacks across the United States. *Science*, *352*(6287), 825–828. doi:10.1126/science.aaa7185

van der Ent, R. J., & Savenije, H. H. (2011). Length and time scales of atmospheric moisture recycling. *Atmospheric Chemistry and Physics*, *11*(5), 1853–1863. doi:10.5194/acp-11-1853-2011

van der Ent, R. J., Savenije, H. H., Schaefli, B., & Steele-Dunne, S. C. (2010). Origin and fate of atmospheric moisture over continents. *Water Resources Research*, *46*(9). doi:10.1029/2010wr009127

van der Ent, R. J., Tuinenburg, O. A., Knoche, H.-R., Kunstmann, H., & Savenije, H. H. (2013). Should we use a simple or complex model for moisture recycling and atmospheric moisture tracking? *Hydrology and Earth System Sciences*, *17*(12), 4869–4884. doi:10.5194/hess-17-4869-2013

van der Ent, R. J., Wang-Erlandsson, L., Keys, P. W., & Savenije, H. H. (2014). Contrasting roles of interception and transpiration in the hydrological cycle – Part 2: Moisture recycling. *Earth System Dynamics*, *5*(2), 471–489. doi:10.5194/esd-5-471-2014

Wang, J., Bai, X., Hu, H., Clites, A., Colton, M., & Lofgren, B. (2012). Temporal and Spatial Variability of Great Lakes Ice Cover, 1973–2010*. *Journal of Climate*, *25*(4), 1318–1329. doi:10.1175/2011jcli4066.1

Wang, Z., Zhan, C., Ning, L., & Guo, H. (2021). Evaluation of global terrestrial evapotranspiration in CMIP6 models. *Theoretical and Applied Climatology*, *143*(1-2), 521–531. doi:10.1007/s00704-020-03437-4

Wang-Erlandsson, L., van der Ent, R. J., Gordon, L. J., & Savenije, H. H. (2014). Contrasting roles of interception and transpiration in the hydrological cycle – Part 1: Temporal characteristics over land. *Earth System Dynamics*, *5*(2), 441–469. doi:10.5194/esd-5-441-2014

Weng, W., Luedeke, M. K., Zemp, D. C., Lakes, T., & Kropp, J. P. (2018). Aerial and surface rivers: downwind impacts on water availability from land use changes in Amazonia. *Hydrology and Earth System Sciences*, *22*(1), 911–927. doi:10.5194/hess-22-911-2018

https://doi.org/10.5194/hess-2021-284
Preprint. Discussion started: 11 June 2021

Hydrology and Earth System Sciences
Open Access
Discussions

Woodhouse, C. A., & Overpeck, J. T. (1998). 2000 Years of Drought Variability in the Central United States. *Bulletin of the American Meteorological Society*, *79*(12), 2693–2714. doi:10.1175/1520-0477(1998)079<2693:yodvit>2.0.co;2

Zambreski, Z. T., Lin, X., Aiken, R. M., Kluitenberg, G. J., & Pielke Sr, R. A. (2018). Identification of hydroclimate subregions for seasonal drought monitoring in the U.S. Great Plains. *Journal of Hydrology*, *567*, 370–381. doi:10.1016/j.jhydrol.2018.10.013